

# *Ab initio* study of electronic states and radiative properties of the AcF molecule

Leonid V. Skripnikov,<sup>1,2,\*</sup> Alexander V. Oleynichenko,<sup>1,†</sup> Andréi Zaitsevskii,<sup>1,3</sup>  
Nikolai S. Mosyagin,<sup>1</sup> Michail Athanasakis-Kaklamanakis,<sup>4,5</sup> Mia Au,<sup>6</sup> and Gerda Neyens<sup>5</sup>

<sup>1</sup>*Petersburg Nuclear Physics Institute named by B.P. Konstantinov of National  
Research Center “Kurchatov Institute” (NRC “Kurchatov Institute” – PNPI),  
1 Orlova roscha, Gatchina, 188300 Leningrad region, Russia*

<sup>2</sup>*Saint Petersburg State University, 7/9 Universitetskaya nab., St. Petersburg, 199034 Russia*

<sup>3</sup>*Department of Chemistry, M.V. Lomonosov Moscow State University, Leninskie gory 1/3, Moscow, 119991 Russia*

<sup>4</sup>*Experimental Physics Department, CERN, CH – 1211 Geneva 23, Switzerland*

<sup>5</sup>*KU Leuven, Instituut voor Kern- en Stralingsfysica, B – 3001 Leuven, Belgium*

<sup>6</sup>*Systems Department, CERN, CH – 1211 Geneva 23, Switzerland*

Relativistic coupled-cluster calculations of the ionization potential, dissociation energy, and excited electronic states under  $35,000\text{ cm}^{-1}$  are presented for the actinium monofluoride (AcF) molecule. The ionization potential is calculated to be  $\text{IP}_e = 48,866\text{ cm}^{-1}$ , and the ground state is confirmed to be a closed-shell singlet and thus strongly sensitive to the  $\mathcal{T}, \mathcal{P}$ -violating nuclear Schiff moment of the Ac nucleus. Radiative properties and transition dipole moments from the ground state are identified for several excited states, achieving an uncertainty of  $\sim 450\text{ cm}^{-1}$  for the excitation energies. For higher-lying states that are not directly accessible from the ground state, possible two-step excitation pathways are proposed. The calculated branching ratios and Franck-Condon factors are used to investigate the suitability of AcF for direct laser cooling. The lifetime of the metastable  $(1)^3\Delta_1$  state, which can be used in experimental searches of the electric dipole moment of the electron, is estimated to be of order 1 ms.

## INTRODUCTION

Radioactive molecules containing heavy atoms provide unique opportunities to search for new physics beyond the Standard model (SM) [1]. The yet undiscovered realm can manifest itself in interactions violating time-reversal ( $\mathcal{T}$ ) and/or parity ( $\mathcal{P}$ ) symmetries [2–6], and the shifts that such interactions induce in the energies of molecular electronic states can be probed in modern tabletop-scale experiments.

There are several key factors that make molecules of heavy-element compounds highly valuable for such experiments. Large internal effective electric fields and the presence of closely spaced levels of opposite parity greatly increase the sensitivity to symmetry-violating interactions (see Refs. [5, 7–9] and references therein). Furthermore, it is possible to design molecules with heavy atoms which can be laser-cooled, resulting in increased coherence times [10–19]. Finally, heavy elements typically have a large number of isotopes with different nuclear properties, some of which have been predicted to possess outstandingly large  $\mathcal{P}$ - and  $\mathcal{T}, \mathcal{P}$ -violating nuclear electromagnetic moments induced by yet unknown nucleon-nucleon interactions [2]. The  $\mathcal{P}$ -violating nuclear anapole moment and the  $\mathcal{T}, \mathcal{P}$ -violating nuclear Schiff and magnetic quadrupole moments are among them. Nuclear structure theory predicts that these moments can be greatly enhanced in octupole deformed nuclei [20–25].

The direct observation of  $\mathcal{T}, \mathcal{P}$ -violating nuclear Schiff moments can help to shed light on the overwhelming imbalance of matter and antimatter in the Universe and the  $\mathcal{CP}$  problem of quantum chromodynamics, both of which

cannot be explained within the SM [5, 26, 27]. Highly sensitive experiments attempting to make the first successful measurement of a nuclear Schiff moment across the nuclear chart can set new limits on the quantum chromodynamics vacuum angle  $\bar{\theta}$  and other hadronic  $\mathcal{CP}$ -violation parameters. The most suitable species for such experiments are diamagnetic atoms and molecules. Thus, several experiments have been performed using Hg [28–30] and Xe [31–33] atoms and the TlF molecule [34–36]. Moreover, a solid-state experiment sensitive [37] to the oscillating nuclear Schiff moment of  $^{207}\text{Pb}$  has been recently performed [38].

Despite the global efforts, no nuclear Schiff moment has been successfully measured so far, and only upper bounds have been placed by the various experiments. To make progress towards a successful measurement, nuclei with enhanced Schiff moments and compounds that are the most sensitive to these moments need to be identified. Recently, a series of diatomic molecules containing octupole-deformed lanthanide and actinide nuclei, namely,  $^{227}\text{AcF}$ ,  $^{227}\text{AcN}$ ,  $^{227}\text{AcO}^+$ ,  $^{229}\text{ThO}$ ,  $^{153}\text{EuO}^+$  and  $^{153}\text{EuN}$ , was proposed [39, 40]. For these molecules, estimated energy shifts [40] arising from the interaction between the nuclear Schiff moment and molecular electrons were predicted to be up to three orders of magnitude greater than in TlF, making these systems promising for the next generation of experimental campaigns. Since a strong enhancement in the nuclear Schiff moment is expected for the  $^{225}\text{Ac}$  and  $^{227}\text{Ac}$  isotopes [24, 41, 42], actinium compounds are highly promising candidates for such experiments.  $^{225}\text{Ac}$  and  $^{227}\text{Ac}$  are rather long-lived with  $T_{1/2} = 10$  days and  $T_{1/2} = 21.8$  years, respectively, and supplies are commercially available as  $^{225}\text{Ac}$  is inves-

tigated for targeted- $\alpha$  cancer therapy [43].

Radioactive nuclides can be produced at accelerator facilities such as ISOLDE at CERN [44] and delivered in the form of radioactive molecular ion beams [45]. Current production techniques involve extraction from a target material and subsequent ionization, and thus benefit from theoretical predictions of molecular properties such as the ionization potential and dissociation energy. Radioactive molecules containing isotopes with half-lives down to a few tens of milliseconds can be produced and studied, as was demonstrated recently with the study of several isotopologues of RaF [46–48] at the CRIS (Collinear Resonance Ionization Spectroscopy) experiment [49, 50]. Both broadband and narrowband collinear laser spectroscopy can be performed, and similar studies are planned on AcF molecules with a multidisciplinary motivation of fundamental, nuclear, and medical physics [51].

No experimental data exist for AcF as of yet, while the available theoretical information is also quite modest. Relativistic coupled cluster calculations [40] predict AcF to have a closed-shell ground state with an equilibrium internuclear distance of  $r_e = 2.12$  Å, and give a preliminary theoretical estimate of its ionization potential (IP), 48,600(250)  $\text{cm}^{-1}$  [51]. Excitation energies for transitions to six excited electronic states were predicted [51], but the picture is not complete since the two-electron excitations with respect to the electronic ground state were not accounted for in the employed theoretical model. Furthermore, no predictions for the transition dipole moments have been made so far, even though they are necessary to locate the strongest transitions and thus to optimally design the first spectroscopic search. Lastly, a theoretical estimate remains to be made regarding the suitability of AcF for direct laser cooling, since the isovalent TlF molecule is predicted to be laser-coolable [52].

Here, we expand the available information about AcF with a comprehensive theoretical study of its electronic structure. Firstly, we re-examine the value of the ionization potential and calculate the dissociation energy. Secondly, we present the general picture of the excited electronic states and their spectroscopic constants. Afterwards, the most promising one- and two-step electronic transitions from the ground state for future spectroscopic measurements are proposed on the basis of the calculated transition dipole moments. Finally, we discuss the laser-coolability of AcF and its possible use in future experiments aimed at searches of  $\mathcal{T}$ ,  $\mathcal{P}$ -violating interactions.

## COMPUTATIONAL METHODS

### Ionization potential calculations

The IP of AcF can be determined as the difference between the total energies of the neutral AcF molecule and

the AcF<sup>+</sup> cation in their electronic ground states (IP<sub>e</sub>), and also with taking into account the zero-vibrational contribution (IP<sub>0</sub>). Since electronic ground-state wavefunctions of AcF and AcF<sup>+</sup> are dominated by a single Slater determinant, the relativistic single-reference coupled-cluster theory (RCC) is the optimal choice to calculate the IP. Within this approach, the exact electronic wave function  $\Psi$  can be written in the exponential form (see e.g. Refs. [53, 54] and references therein for a comprehensive review of the CC theory):

$$|\Psi\rangle = e^{\hat{T}} |\Phi_0\rangle, \quad \hat{T} = \hat{T}_1 + \hat{T}_2 + \hat{T}_3 + \dots \quad (1)$$

where  $\Phi_0$  is the reference determinant and the cluster operator  $T$  consists of  $n$ -body terms representing single ( $\hat{T}_1$ ), double ( $\hat{T}_2$ ), triple ( $\hat{T}_3$ ), etc. excitations with respect to  $\Phi_0$ . The basic CCSD model necessarily includes only single and double excitation operators ( $\hat{T} \approx \hat{T}_1 + \hat{T}_2$ ), and various approximate schemes accounting for higher excitations have been developed.

The simplest and least computationally demanding approach to account for triple excitations is the CCSD(T) model, which involves the solution of the CCSD equations followed by the non-iterative calculation of the approximate fifth-order perturbation correction arising from connected triples [55]. The more sophisticated CCSDT-3 model also estimates the triple-excitation amplitudes perturbatively, but they are now included into the iterative solution of equations for the  $\hat{T}_1$  and  $\hat{T}_2$  amplitudes [56]. Even better level of accuracy is attained within the full CCSDT model [57], which treats the  $\hat{T}_3$  operator in a fully consistent iterative manner without any additional neglects and approximations. Contributions from the quadruple-excitation operator  $\hat{T}_4$  can be accounted for within corresponding similar approximations CCSDT(Q) and CCSDTQ-3 [58, 59]. It must be noted, however, that the computational cost grows very quickly when going from CCSD(T) to CCSDTQ-3.

To calculate the IP and the dissociation energy ( $D_e$ ) of AcF, the following computational scheme was used. The leading-order value was obtained within the relativistic CCSD(T) approach using the Dirac-Coulomb Hamiltonian. Here, 70 electrons of AcF were included in the correlation treatment. The virtual molecular orbital energy cutoff was set to 300 Hartree. The MBas basis set was employed, corresponding to the extended uncontracted all-electron triple-zeta Dyall’s AETZ [60, 61] basis set for Ac and the uncontracted augmented all-electron quadruple-zeta AAEQZ [62–64] basis set for F.

Higher-order correlation effects were accounted for with a scheme of incremental corrections. The first correction was calculated as the difference between the IP ( $D_e$ ) values calculated at the CCSDT-3 and CCSD(T) levels, with both calculations performed with 38 correlated electrons and the two-component generalized relativistic pseudopotential (GRPP) model [65–68] for the

Hamiltonian. At this stage, the energy cutoff for virtual orbitals was set to 35 Hartree and a compact basis set (CBas) of atomic natural orbitals was generated using the procedure developed and described in Refs. [69, 70]. The basis set for Ac thus consisted of  $8s$ -,  $8p$ -,  $7d$ -,  $4f$ -,  $4g$ - and  $2h$ -type contracted functions and can be denoted as  $(20s20p20d15f15g15h)/[8s8p7d4f4g2h]$ , where the numbers in the ()-brackets are the numbers of primitive Gaussian functions included in the contracted functions listed in the []-brackets. The aug-cc-pVTZ-DK basis set [71–73] was used for F.

The next correlation correction included the difference between the IP values obtained within the CCSDT and CCSDT-3 approaches. Due to the very high computational cost of the CCSDT model, only 28 electrons of AcF were correlated and the basis set used was further reduced to  $(20s20p20d15f)/[8s8p7d4f]$  for Ac and aug-cc-pVDZ-DK set [71–73] for F; we call this basis set SBas. The virtual energy cutoff was set to 10 Hartree. To derive the contribution of connected quadruple-cluster amplitudes, we calculated the difference between IP values obtained within the CCSDT(Q) and CCSDT approaches using the similar parameters as in the “CCSDT – CCSDT-3” correction, except that the virtual orbitals energy cutoff was set to 5 Hartree. The last correction for even higher-order correlation effects was obtained as the difference between the CCSDTQ-3 and CCSDT(Q) values, correlating the 18 outermost electrons. In this calculation, the virtual orbital energy cutoff was reduced to 4 Hartree and the Ac basis set was reduced to  $(20s20p20d15f)/[8s6p5d3f]$ . Similar corrections were also used to calculate  $D_e$ .

To account for the incompleteness of the basis set, corrections to the IP and  $D_e$  were calculated using the scalar-relativistic part of the GRPP operator. Such a simplification of the Hamiltonian allowed us to employ a very large basis set (LBas) consisting of  $[30s30p30d30f15g15h15i]$  uncontracted basis functions for Ac and the extended Dyall’s uncontracted AAEQZ [64] set for F. In the latter case, we replaced the original basis functions of the AAEQZ basis with  $l = 3, 4, 5, 6$  by corresponding functions of the aug-cc-pV7Z [74] basis set. The basis set correction was thus calculated as the difference between the CCSD(T) values of the IP obtained using the LBas versus the MBas basis sets, including 38 AcF electrons in the correlation treatment.

The contribution of the Gaunt electron-electron interaction was estimated using the molecular-mean-field exact two-component approach [75] at the Fock-space RCCSD (FS-RCCSD) level. Finally, the contribution of quantum electrodynamics (QED) effects was taken into account using the model QED Hamiltonian approach [76, 77] adapted for molecular calculations [78].

Relativistic calculations of the IP and  $D_e$  were carried out using the DIRAC [79, 80] and MRCC [81–84] packages.

Scalar relativistic correlation calculations were performed using the CFOUR [85, 86] code.

### Excited-state calculations

Qualitatively, the electronic states of AcF can be regarded as the states of  $\text{Ac}^+$  split by the field of the  $\text{F}^-$  anion. The atomic spectrum of  $\text{Ac}^+$  is dense, with several dozens of states observed below  $\sim 50,000 \text{ cm}^{-1}$  [87]. In the energy range below  $30,000 \text{ cm}^{-1}$ , the  $\text{Ac}^+$  states are dominated by the  $7s^2$ ,  $7s6d$ ,  $6d^2$ ,  $7s7p$ , and  $7p6d$  configurations, while for higher-lying states the  $7s5f$ ,  $7s8s$ , and  $6d5f$  configurations are the leading ones. These patterns are generally inherited by the AcF molecule, resulting in a very dense spectrum of electronic states. For this reason, the electronic structure of AcF is strikingly different from that of TlF, which can be considered as an isovalent molecule. In contrast to Ac, one of the valence  $s$ -electrons ( $6s$  electron in this case) of Tl never participates in low-energy excitations [88–90].

The general feature of the majority of excited electronic states in AcF is their multireference character, meaning that no single determinant dominates the expansion of the electronic wave function. Therefore, the scheme used to calculate the IP based on the single-reference approximation cannot be applied to the excited states. The typical method of choice to solve such problems is the relativistic multireference Fock space coupled cluster theory (FS-RCC) [91–93]. This approach is again based on the exponential parametrization of the many-electron wavefunction, but in contrast to Eq. (1), exact wavefunctions  $\Psi_i$  are obtained by acting on model vectors  $\tilde{\Psi}_i$ :

$$|\Psi_i\rangle = \{e^T\} |\tilde{\Psi}_i\rangle, \quad |\tilde{\Psi}_i\rangle = \sum_m C_{im} |\Phi_m\rangle. \quad (2)$$

The model vectors represent the leading terms in the expansions of full electronic wavefunctions and are constructed from the model-space Slater determinants  $\Phi_m$ . The two-particle Fock-space sector ( $0h2p$ ) determinants  $\Phi_m$  used in the present paper are obtained from the Fermi vacuum determinant  $\Phi_0$  (the  $0h0p$  sector) by adding two electrons and distributing them in chosen *active* one-particle spinors in all possible ways. The cluster operator  $\hat{T}$  is also extended to enable electronic excitations from these active spinors.

In order to be able to consider very large model spaces required for a reasonable description of the multireference problem and to avoid convergence difficulties arising from the intruder-state problem that is typical for FS-RCC, formulations based on the intermediate Hamiltonian (IH) concept were developed (see [93] and references therein). Among these formulations, the version that operates with incomplete main model spaces [94] seems to be the most powerful. In this case, the whole model space

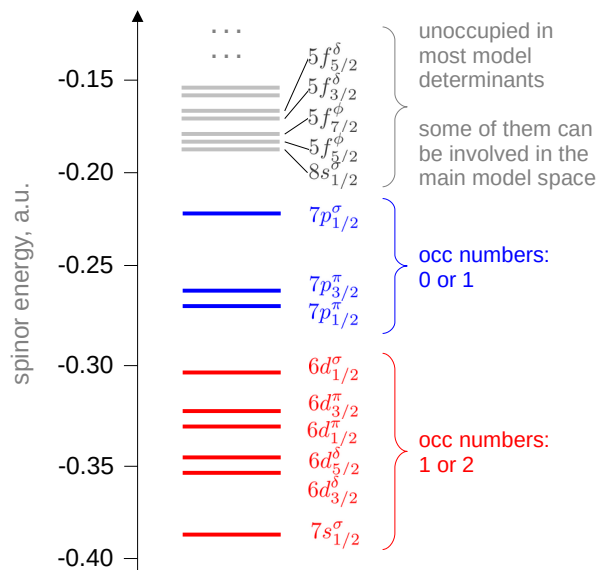


FIG. 1. Energy diagram for active space of one-electron spinors of the  $\text{AcF}^{2+}$  ion (the upper part is not shown). To define the incomplete main model space in the IH technique the active space is divided into three parts.

for a given Fock-space sector is split into the main and auxiliary intermediate subspaces. The most accurate description that is stable with respect to the IH parameters is achieved for the states dominated by *main* model subspace determinants (see Ref. [94] for the details of the IH formulation for the incomplete main-model space used here).

For  $\text{AcF}$ , the excited electronic states of interest can be best described within the IH-FS-RCC approach starting from the Fermi vacuum that corresponds to the closed-shell  $\text{AcF}^{2+}$  cation. Note that the essentially two-electron nature of excitations from the closed-shell ground state prevents the use of FS-RCC in the one hole, one particle ( $1h1p$ ) sector to describe the majority of states of  $\text{AcF}$  below  $50,000 \text{ cm}^{-1}$ . However, auxiliary IH-FS-RCCSD( $1h1p$ ) calculations allowed us to conclude that charge-transfer states dominated by excitations from the  $p$ -shells of the F atom lie at energies  $\sim 72,000 \text{ cm}^{-1}$ , which is well above the IP value of  $48,866 \text{ cm}^{-1}$  obtained in the present work.

The qualitative picture of the  $\text{AcF}$  electronic states that is described above also allows one to conveniently classify one-electron molecular spinors of  $\text{AcF}^{2+}$  and to properly construct the main-model subspace for the IH-FS-RCC calculation. Overall, the 49 lowest-energy Kramers pairs of virtual spinors of  $\text{AcF}^{2+}$  comprised the active space, which was further divided into three parts, as shown in Fig. 1.

The first part comprised the lowest-lying  $7s_{1/2}^{\sigma}$ ,  $6d_{3/2}^{\delta}$ ,  $6d_{5/2}^{\delta}$ ,  $6d_{1/2}^{\pi}$ ,  $6d_{3/2}^{\pi}$  and  $6d_{1/2}^{\sigma}$  spinors. Here, the  $7s_{1/2}^{\sigma}$  spinor refers to the molecular  $\sigma_{1/2}$  spinor arising mainly

from the  $7s$  atomic orbital of  $\text{Ac}^{2+}$ , etc. Model-space determinants bearing one or two electrons on these spinors were considered as belonging to the main subspace. The second block of active spinors included  $7p_{1/2}^{\pi}$ ,  $7p_{3/2}^{\pi}$  and  $7p_{1/2}^{\sigma}$  spinors, and the configurations with maximum one electron on them were also treated as the main ones. The maximum of zero-order energies of these “main” configurations was considered as the frontier energy which was then used to calculate the energy denominator shift parameters used in the IH-FS-RCC scheme (see Ref. [94] for technical details). Finally, all the remaining active spinors served to construct intermediate “buffer” determinants that were not included in the main model subspace. However, configurations with energies below the frontier energy, including  $7s_{1/2}^{\sigma}8s_{1/2}^{\sigma}$  and  $7s_{1/2}^{\sigma}5f$ , were also added to the main subspace (despite the fact that the  $8s_{1/2}^{\sigma}$  and  $5f$  spinors belong to the third subspace in Fig. 1) as they are necessary to maintain the correct physical picture. Such a composition of the incomplete main-model space allows us to reach nearly all electronic states below  $\sim 43,000 \text{ cm}^{-1}$ ; states above this energy received significant contributions from “buffer” determinants and are thus expected to be described less accurately.

The IH-FS-RCCSD model with single and double excitations in the cluster operator was used for the excited-state calculations. To reduce systematic errors dependent on the internuclear separation and arising from the neglect of higher cluster amplitudes and basis set incompleteness, we combined excitation energies computed within the IH-FS-RCCSD model with the ground-state potential energy curve obtained at the CCSD(T) level (as it was previously done in Refs. [95–97]). The counterpoise correction was applied to reduce the basis set superposition error. All molecular spinors up to the virtual energy cutoff of 300 Hartree were included in the correlation calculations.

Relativistic (including the Breit electron-electron interaction) and QED effects were effectively simulated using the generalized relativistic pseudopotential (GRPP) operator [65, 67, 94, 98], whose high accuracy for actinide compounds has been previously demonstrated [97, 99]. The new tiny-core GRPP for Ac, replacing 28 core electrons and accounting for the Breit interaction, finite-nuclear-size, and QED contributions (electron self-energy and vacuum polarization [76, 100]), was constructed [101]. Atomic low-lying excitation energies calculated for the neutral Ac atom and its  $\text{Ac}^{+}$  cation at the relativistic two-component Hartree-Fock level with GRPP deviate from the reference all-electron Dirac-Coulomb-Breit + QED results by a few wavenumbers. These deviations do not exceed  $20 \text{ cm}^{-1}$  even for the  $5f$  states of  $\text{Ac}^{+}$  (see Supplementary Materials), whereas the contributions from Breit interactions and QED effects reach  $500$  and  $200 \text{ cm}^{-1}$ , respectively. For the F atom, the empty-core GRPP that leaves all 9 electrons



for explicit treatment and thus simulates only relativistic effects [102] was employed.

The basis set for Ac in the IH-FS-RCCSD calculations was based on the quadruple-zeta Dyall’s basis set [60, 61] and was comprised of the (21s16p17d15f8g6h4i) primitive Gaussian functions. For the F atom, the uncontracted version of the Dyall’s AAEQZ basis set [64] was employed. Such an extensive basis set ensures a high computational quality for a broad manifold of AcF electronic states, including those bearing the 8s and 5f electrons of Ac.

Transition dipole moments (TDMs) were calculated using the direct finite-order approach based on the substitution of the exponential wave operator into bra- and ket-vectors, and the infinite summation was truncated at terms quadratic in cluster amplitudes ([97]; see also Ref. [103–107] for the analogous technique in atomic calculations). This approach allows one to obtain TDMs for all pairs of electronic states simultaneously. In contrast to the finite-field (FF) technique [108, 109], it does not require any reduction in the molecular symmetry to calculate TDMs for the  $\Delta\Omega = \pm 1$  case. To verify the accuracy of TDM calculations, the  $0^+ - 0^+$  transition moments were also evaluated using the FF method for which the typical error is expected to be within few percent [109–111]. Radiative decay rates and lifetimes of excited rovibrational states were evaluated using the Tellinghuisen’s sum rule [112].

Single-reference relativistic CCSD(T) calculations as well as solutions of the relativistic Hartree-Fock equations with subsequent integral transformation were obtained using the DIRAC package [79, 80] supplemented by the LIBGRPP module [99, 113] to evaluate molecular integrals over generalized pseudopotentials. Excitation energies and TDMs were obtained within the EXP-T program package [114, 115]. Molecular integrals over the operator of the projection of the electronic orbital angular momentum on the molecular axis  $L_z$  that are required to calculate its expectation values were calculated using the OneProp code [116]. To solve the one-dimensional vibrational problem and calculate lifetimes, the VIBROT program [117] was used. Vibrational constants  $\omega_e$  for each potential were derived from the first three calculated vibrational levels.

## RESULTS AND DISCUSSION

### Ionization potential and dissociation energy of AcF

Contributions to the IP of AcF are given in Table I. It is evident that correlation effects beyond the CCSD(T) model contribute quite significantly to the IP value, though they partly compensate for each other.

Connected quadruple excitations that firstly appear in the CCSDT(Q) approach contribute about  $+166 \text{ cm}^{-1}$ ,

TABLE I. Calculated ionization potential and dissociation energy of AcF. The total correlation correction summarizes the contributions of correlation effects beyond the CCSD(T) model.

Contribution	IP, $\text{cm}^{-1}$	$D$ , $\text{cm}^{-1}$
CCSD(T)	49,083	57,209
CCSDT-3 – CCSD(T)	–246	63
CCSDT – CCSDT-3	–93	–347
CCSDT(Q) – CCSDT	166	–24
CCSDTQ-3 – CCSDT(Q)	–51	61
Total correlation correction	–224	–247
Basis set correction	91	308
QED	–51	–24
Gaunt	–32	–32
Zero-vibrational energy	33	–269
Total, IP <sub>e</sub> and $D_e$	48,866	57,214
Total, IP <sub>0</sub> and $D_0$	48,898	56,946

while the CCSDTQ-3 model further corrects the IP value by  $-51 \text{ cm}^{-1}$ . Contributions of the QED and Gaunt interaction effects were found to be quite small,  $-51$  and  $-32 \text{ cm}^{-1}$ , respectively. **The final value for the IP<sub>e</sub> is 48,866(130)  $\text{cm}^{-1}$**  (see Supplementary Materials for details of the employed scheme for the uncertainty estimation).

It should be noted that the IP<sub>e</sub> value was calculated as the difference of ground state electronic energies of the AcF<sup>+</sup> cation and AcF molecule. These energies were obtained in separate single-reference CC calculations with different Fermi-vacuum states. The precise experimental measurement of the IP will be able to probe the accuracy of this theoretical prediction, and it is thus valuable for testing the accuracy of the ground-state electronic wavefunctions of AcF<sup>+</sup> and AcF. As it was mentioned in the Introduction, the electronic ground state of AcF can be used as a working state to measure the Schiff moment of the Ac nucleus. An accurate interpretation of such an experiment will require the knowledge of the molecular enhancement constant that is determined by the ground-state electronic wavefunction of AcF. Although there is no explicit relation between IP<sub>e</sub> and the Schiff moment molecular enhancement, a good agreement between theoretical and experimental values for the IP is important to establish the reliability of electronic structure calculations.

The upcoming experimental campaign by the CRIS collaboration [51] also aims at an accurate determination of  $D_e$  in AcF. Both the IP and  $D_e$  are critical values for ionization processes during which dissociation can also occur, affecting the production

techniques of actinium isotopes, including the medical radioisotope  $^{225}\text{Ac}$ . From the experimental data on the Ac ionization potential and F electron affinity [87], it follows that the ionic decay channel  $\text{AcF} \rightarrow \text{Ac}^+ (^1S_0) + \text{F}^- (^1S_0)$  lies  $15,962 \text{ cm}^{-1}$  above the neutral channel  $\text{AcF} \rightarrow \text{Ac} (^2D_{3/2}) + \text{F} (^2P_{3/2}^o)$ . Therefore, the latter channel is considered. Obtained contributions to the dissociation energy of AcF are given in Table I. One can see a slightly different contribution pattern compared to the IP case, though in both cases correlation effects beyond the CCSD(T) model have quite small contributions that partly compensate for each other. **The final value for the  $D_e$  is thus  $57,214(234) \text{ cm}^{-1}$ .**

### Excited electronic states in AcF

The potential energy curves of the AcF molecule shown in Fig. 2 were calculated for the range of internuclear separations from 3.60 a.u. (1.905 Å) to 4.40 a.u. (2.328 Å). The chosen range is large enough to ensure the accurate numerical evaluation of wavefunctions and energies of at least the three lowest vibrational levels for each of the considered electronic states. The energy range up to  $\sim 43,000 \text{ cm}^{-1}$  is limited by the composition of the main model space adopted in the present calculation. Spectroscopic constants including term energies  $T_e$ , equilibrium internuclear distances  $r_e$ , and vibrational constants  $\omega_e$  for the states below  $35,000 \text{ cm}^{-1}$  are summarized in Table II.

The IH-FS-RCCSD calculations confirm previously published predictions [40, 51] that the electronic ground state is a closed-shell singlet with  $\Omega = 0^+$ . Potential energy curves for most of the considered electronic states are nearly parallel to each other, with  $r_e$  lying well between 2.1 and 2.2 Å, indicating that the electronic excitations are localized at the Ac atom as expected. The general pattern of potential energy curves closely resembles those of other actinide-containing diatomic molecules (for example, ThO [97], ThF<sup>+</sup> [118], and PaF<sup>3+</sup> [18]). The density of electronic states rapidly grows for the energy range above  $\sim 30,000 \text{ cm}^{-1}$ , resulting in a very complicated picture with many avoided crossings. This energy range does not seem to be convenient for experimental studies, since a firm interpretation of observed transitions would be hardly possible without the construction of comprehensive non-adiabatic rovibronic models [119, 120], which in turn require a large amount of spectroscopic data to be reliable. For the same reason, one can expect a substantially perturbed vibronic spectrum for transitions involving the (6)1  $\sim$  (7)1 and (4)2  $\sim$  (5)2 complexes (see Fig. 2b and 2c).

To better understand the structure of AcF, it is useful to represent the relativistic molecular electronic states in terms of their scalar-relativistic ( $\Lambda - S$ ) counterparts. To perform such an analysis, an additional IH-FS-RCCSD

calculation with the spin-orbit parts of pseudopotentials nearly switched off was performed for the point  $r = 4.0 \text{ a.u.} = 2.117 \text{ Å}$  that is close to the equilibrium distance in the majority of the studied AcF electronic states. The model-space parts of the obtained scalar relativistic states were then projected onto the manifold of fully relativistic states (see [121] for details). The results are summarized in Tab. II. For the majority of states presented in Tab. II, compositions in terms of  $\Lambda - S$  states are far from pure, which is also illustrated by the expectation values of the  $L_z$  operator. This observation clearly emphasizes the important role of the spin-orbit interaction in this system.

Such an analysis also sheds light onto the nature of the (6)1  $\sim$  (7)1 and (4)2  $\sim$  (5)2 complexes. The avoided crossing in the former (see Fig. 2b) arises from the spin-orbit interaction between the  $(2)^3\Sigma^-$  and  $(2)^1\Pi$  components that dominate these states and is thus characteristic of a purely relativistic picture. The situation is similar for the (4)2  $\sim$  (5)2 complex (see Fig. 2c), since these two states are strongly dominated by the  $(1)^3\Phi$  and  $(2)^3\Pi$  scalar-relativistic states, respectively. In both of these cases, the crossing points lie close to  $r_e$ , resulting in the necessity to construct non-adiabatic models to treat their rovibrational structure. Such models are typically constructed with the involvement of a large amount of experimental data [119, 120]. This seems to be unrealistic at the present level of theory. The avoided crossing also exists between the (8)1 and (9)1 states at  $r \approx 2.3 \text{ Å}$ , but it is expected that few unperturbed vibrational states exist for the (8)1 potential. In this case, the avoided crossing also stems from the spin-orbit coupling, mainly between the  $(2)^3\Delta$  and the mixture of the  $(2)^1\Pi$  and  $(3)^3\Pi$  states.

It is important to estimate the typical uncertainty of the term energies  $T_e$  given in Table II. The suggested empirical rule is that for FS-RCCSD calculations, the error in the ionization potential hardly exceeds the errors in excitation energies. For AcF, the IH-FS-RCCSD value of the IP equals to  $49,170 \text{ cm}^{-1}$ , which is  $324 \text{ cm}^{-1}$  higher than the more accurate value obtained within the single-reference approach including triple and quadruple excitations ( $48,866 \text{ cm}^{-1}$ ). Taking into account the uncertainty of the latter ( $130 \text{ cm}^{-1}$ ), the uncertainty estimate for the excitation energies is  $\sim 450 \text{ cm}^{-1}$ . This value agrees well with the recently reported errors of IH-FS-RCCSD for the ThO molecule (which has a fairly similar electronic structure) at  $< 400 \text{ cm}^{-1}$  with a root-mean-squared deviation  $280 \text{ cm}^{-1}$  [97]. The bulk of this uncertainty is expected to be due to the absence of triple excitations in the cluster operator. It is worth noting that the uncertainty is comparable to  $\omega_e$  values, thus the present accuracy can be insufficient for an unambiguous assignment of experimentally measured vibrational bands.

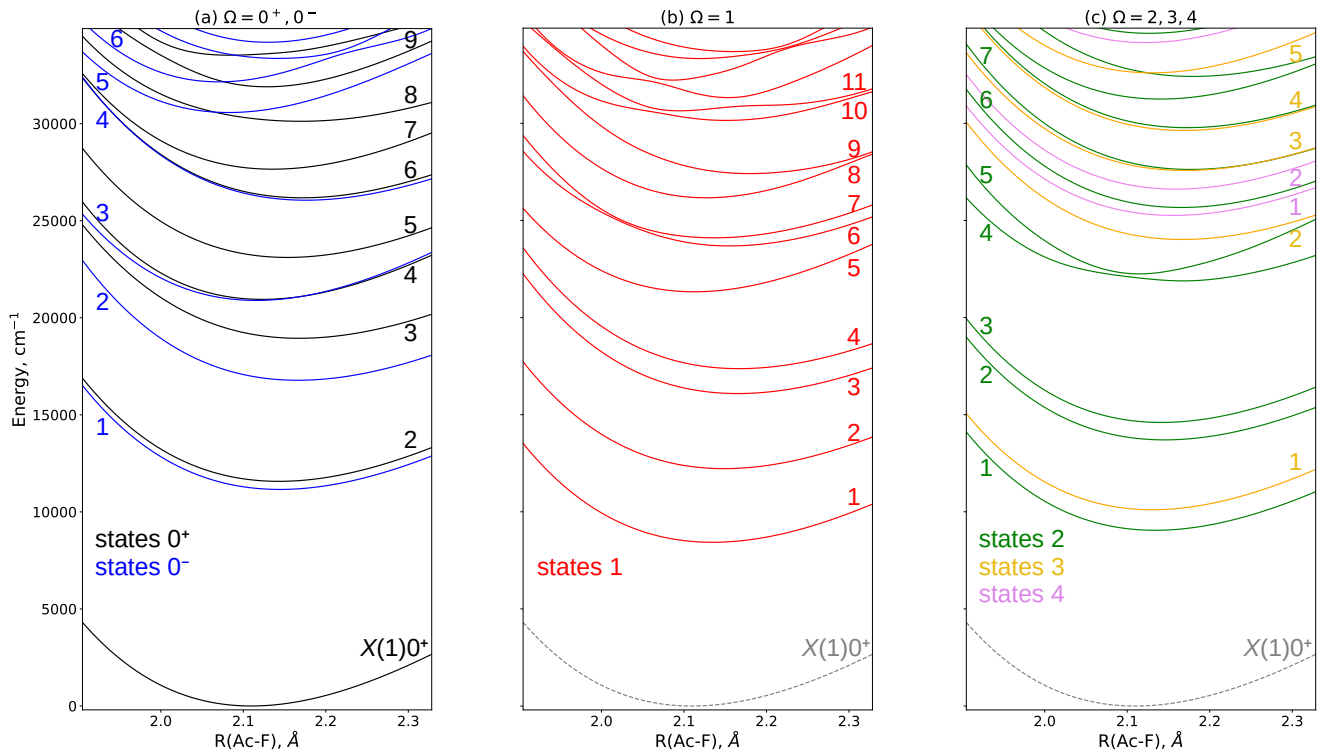


FIG. 2. Potential energy curves of the AcF molecule in different electronic states: (a)  $\Omega = 0^+, 0^-$ ; (b)  $|\Omega| = 1$ ; (c)  $|\Omega| = 2, 3, 4$ . Energies are given with respect to the ground state equilibrium point.

### Radiative properties of ground and excited states

The planned CRIS experiment on AcF at ISOLDE operates with radioactive ion beams at very low intensity (due to a typical production rate of  $\sim 10^6$  molecules/s or lower [45]). Therefore, the identification of the most intense transitions is crucial. The probability of absorption of a photon in the  $E1$  approximation is proportional to the square of the TDM  $|d|^2$ . Since the potential energy curves of excited states are roughly parallel to that of the ground state, and  $r_e$  changes only slightly during the excitation, it is natural to compare intensities of vertical transitions (see Table II). The scheme in Fig. 3 depicts the strongest transitions from the ground state and secondary stimulated emission transitions (discussed below). Based on the obtained data, we expect only three intense transitions to  $\Omega = 0^+$  states,  $(3)0^+$ ,  $(8)0^+$ ,  $(9)0^+$ , and five transitions to  $|\Omega| = 1$  states,  $(3)1$ ,  $(4)1$ ,  $(6)1 \sim (7)1$ ,  $(8)1$ ,  $(10)1$ . Clear unperturbed vibrational progressions could be expected for all these states except for the  $(6)1 \sim (7)1$  spin-orbit-coupled complex and the  $(10)1$  state that belongs to the complex of several states at  $\sim 30,000 - 34,000 \text{ cm}^{-1}$ . TDM functions for the most intense transitions are given in Figs. 4 and 5.

For the  $(6)1 \sim (7)1$  and  $(8)1 \sim (9)1$  complexes, it seems more natural to pass from adiabatic states to their diabatic “spectroscopic” counterparts (see, for example,

Refs. [97, 110, 111] for details), which can be approximately identified with the dominating  $\Lambda - S$  states (see Tab. II). The exact diabaticization can be rather cumbersome. However, in these two particular cases one can use the assumption that the lowest  $X(1)0^+$  state is approximately a pure singlet state. As a result, the quasi-adiabatic  $X0^+ - (2)^1\Pi$  TDM function can be obtained by the requirement of vanishing the formally spin-forbidden  $X0^+ - (2)^3\Sigma^-$  and  $X0^+ - (3)^3\Pi$  transitions; the same holds for the  $(8)1 \sim (9)1$  complex. This simple approach is not valid for transitions to these complexes from many other states. For this reason, we further estimate total probabilities of transitions to the whole complex from higher-lying states without diabaticization. This does not distort the calculated partial lifetimes significantly if the gap between the components of the complex is much smaller than the transition energy.

Additionally, it is found that the probabilities of direct one-photon transitions from the  $X0^+$  state to the manifold of excited states above  $\sim 35,000 \text{ cm}^{-1}$  are rather small, with  $|d|^2 < 0.1$  a.u. However, two-step excitation schemes from the ground state that use different intermediate states can be devised. Table III summarizes the estimates of  $|d|^2$  for such secondary vertical excitations. However, it must be noted that these data should be considered as quite approximate. The  $|d|^2$  values should thus be interpreted as indicative of the presence of a transition to a state with a certain  $|\Omega|$ . Note

TABLE II. Spectroscopic constants of  $^{227}\text{AcF}$  in different electronic states calculated at the IH-FS-RCCSD level.  $|d|^2$  stands for the squared transition dipole moment for transitions from the  $(1)0^+$  ground state. The values for  $\langle L_z \rangle$ ,  $|d|^2$ , the compositions in terms of  $\Lambda S$ -states, and the leading configurations were calculated at  $r(\text{Ac-F}) = 4.0$  a.u. = 2.117 Å.  $\omega_e$  values are absent for the states where the Born-Oppenheimer approximation is not applicable.

State	$T_e$ , $\text{cm}^{-1}$	$r_e$ , Å	$\omega_e$ , $\text{cm}^{-1}$	$ d ^2$ , a.u.	$\langle L_z \rangle$ , a.u.	Composition	Leading configurations
(1)0 <sup>+</sup>	0	2.110	541	–	0.0	100% $X(1)^1\Sigma^+$	92% $7s_{1/2}^\sigma 7s_{1/2}^\sigma$
(2)0 <sup>+</sup>	11574	2.143	503	0.170	0.0	94% $(1)^3\Pi$	88% $7s_{1/2}^\sigma 6d_{1/2}^\pi$ 10% $7s_{1/2}^\sigma 7p_{1/2}^\pi$
(3)0 <sup>+</sup>	18944	2.168	479	2.145	0.0	78% $(2)^1\Sigma^+ + 15\% (2)^3\Pi$	72% $7s_{1/2}^\sigma 6d_{1/2}^\pi$ 10% $6d_{3/2}^\delta 6d_{3/2}^\delta$
(4)0 <sup>+</sup>	20949	2.123	532	0.305	0.0	81% $(2)^3\Pi + 14\% (2)^1\Sigma^+$	76% $7s_{1/2}^\sigma 7p_{1/2}^\pi$
(5)0 <sup>+</sup>	23109	2.153	494	0.286	0.0	75% $(2)^3\Sigma^- + 12\% (3)^1\Sigma^+$	54% $6d_{3/2}^\delta 6d_{3/2}^\delta$ 16% $6d_{5/2}^\delta 6d_{5/2}^\delta$
(6)0 <sup>+</sup>	26182	2.171	479	0.000	0.0	90% $(3)^3\Pi + 8\% (2)^3\Sigma^-$	74% $6d_{3/2}^\delta 6d_{3/2}^\delta$
(7)0 <sup>+</sup>	27656	2.136	503	0.246	0.0	85% $(3)^1\Sigma^+ + 12\% (2)^3\Sigma^-$	60% $6d_{5/2}^\delta 6d_{5/2}^\delta$
(8)0 <sup>+</sup>	30124	2.169	401	0.862	0.0	49% $(4)^1\Sigma^+ + 40\% (4)^3\Sigma^-$	40% $6d_{1/2}^\pi 6d_{1/2}^\pi$ 32% $7s_{1/2}^\sigma 7p_{1/2}^\pi$
(9)0 <sup>+</sup>	31902	2.128	580	1.122	0.0	50% $(4)^1\Sigma^+ + 39\% (4)^3\Sigma^-$	42% $7s_{1/2}^\sigma 7p_{1/2}^\pi$ 18% $6d_{3/2}^\delta 6d_{3/2}^\delta$
(10)0 <sup>+</sup>	33529	2.084	–	0.002	0.0	52% $(5)^1\Sigma^+ + 40\% (4)^3\Pi$	40% $6d_{3/2}^\delta 7p_{3/2}^\pi$ 28% $7s_{1/2}^\sigma 8s_{1/2}^\sigma$
(1)0 <sup>-</sup>	11156	2.144	502	–	0.0	85% $(1)^3\Pi + 13\% (1)^3\Sigma^-$	86% $7s_{1/2}^\sigma 6d_{1/2}^\pi$
(2)0 <sup>-</sup>	16781	2.166	487	–	0.0	82% $(1)^3\Sigma^- + 14\% (1)^3\Pi$	90% $7s_{1/2}^\sigma 6d_{1/2}^\pi$
(3)0 <sup>-</sup>	20895	2.115	532	–	0.0	94% $(2)^3\Pi$	86% $7s_{1/2}^\sigma 7p_{1/2}^\pi$
(4)0 <sup>-</sup>	26058	2.176	473	–	0.0	99% $(3)^3\Pi$	80% $6d_{3/2}^\delta 6d_{3/2}^\delta$
(5)0 <sup>-</sup>	30575	2.082	540	–	0.0	98% $(3)^3\Sigma^-$	84% $7s_{1/2}^\sigma 7p_{1/2}^\pi$
(6)0 <sup>-</sup>	32155	2.070	589	–	0.0	97% $(5)^3\Sigma^-$	84% $7s_{1/2}^\sigma 8s_{1/2}^\sigma$
(7)0 <sup>-</sup>	33363	2.143	–	–	0.0	72% $(4)^3\Pi + 19\% (6)^1\Sigma^+$	50% $6d_{3/2}^\delta 7p_{3/2}^\pi$ 20% $6d_{1/2}^\pi 6d_{1/2}^\pi$
(8)0 <sup>-</sup>	34196	2.130	559	–	0.0	33% $(6)^1\Sigma^+ + 25\% (4)^3\Pi$	34% $6d_{1/2}^\pi 7p_{1/2}^\pi$ 28% $6d_{3/2}^\delta 7p_{3/2}^\pi$
(1)1	8430	2.135	514	0.001	2.0	99% $(1)^3\Delta$	97% $7s_{1/2}^\sigma 6d_{3/2}^\delta$
(2)1	12222	2.149	499	0.244	0.9	78% $(1)^3\Pi + 14\% (1)^3\Sigma^-$	68% $7s_{1/2}^\sigma 6d_{1/2}^\pi$ 16% $7s_{1/2}^\sigma 6d_{3/2}^\delta$
(3)1	16087	2.165	489	0.752	0.6	44% $(1)^3\Sigma^- + 33\% (1)^1\Pi$	49% $7s_{1/2}^\sigma 6d_{3/2}^\delta$ 35% $7s_{1/2}^\sigma 6d_{1/2}^\pi$
(4)1	17369	2.167	487	0.766	0.6	59% $(1)^1\Pi + 39\% (1)^3\Sigma^-$	53% $7s_{1/2}^\sigma 6d_{1/2}^\pi$ 18% $7s_{1/2}^\sigma 6d_{3/2}^\delta$
(5)1	21327	2.113	529	0.195	1.0	90% $(2)^3\Pi + 6\% (2)^1\Pi$	58% $7s_{1/2}^\sigma 7p_{1/2}^\pi$ 22% $7s_{1/2}^\sigma 7p_{3/2}^\pi$
(6)1	23688	2.155	–	0.027	0.2	91% $(2)^3\Sigma^- + 6\% (3)^3\Pi$	78% $6d_{3/2}^\delta 6d_{5/2}^\delta$
(7)1	24105	2.137	–	1.706	1.1	49% $(2)^1\Pi + 21\% (3)^3\Pi$	31% $6d_{3/2}^\delta 6d_{1/2}^\pi$ 29% $7s_{1/2}^\sigma 7p_{3/2}^\pi$
(8)1	26166	2.127	549	3.751	1.1	42% $(2)^1\Pi + 30\% (3)^3\Pi$	21% $7s_{1/2}^\sigma 7p_{3/2}^\pi$ 19% $7s_{1/2}^\sigma 7p_{1/2}^\pi$
(9)1	27412	2.180	469	0.005	1.6	65% $(2)^3\Delta + 31\% (3)^3\Pi$	67% $6d_{3/2}^\delta 6d_{1/2}^\pi$
(10)1	30150	2.151	–	0.815	1.0	87% $(3)^1\Pi + 8\% (3)^3\Pi$	48% $6d_{5/2}^\delta 6d_{3/2}^\delta$ 9% $6d_{3/2}^\delta 6d_{1/2}^\pi$
(11)1	30643	2.094	–	0.120	0.1	89% $(3)^3\Sigma^- + 6\% (4)^3\Sigma^-$	77% $7s_{1/2}^\sigma 7p_{1/2}^\pi$
(12)1	31324	2.154	–	0.001	0.1	86% $(4)^3\Sigma^- + 7\% (3)^3\Sigma^-$	69% $6d_{1/2}^\pi 6d_{3/2}^\delta$
(13)1	32224	2.087	–	0.019	0.0	98% $(5)^3\Sigma^-$	84% $7s_{1/2}^\sigma 8s_{1/2}^\sigma$
(14)1	33334	2.119	–	0.218	1.0	66% $(4)^3\Pi + 29\% (4)^1\Pi$	62% $6d_{3/2}^\delta 7p_{1/2}^\pi$
(15)1	33694	2.160	–	0.001	1.8	81% $(3)^3\Delta + 8\% (5)^3\Pi$	59% $6d_{1/2}^\pi 7p_{1/2}^\pi$ 20% $6d_{1/2}^\pi 6d_{1/2}^\pi$
(1)2	9048	2.134	514	–	2.0	96% $(1)^3\Delta$	66% $7s_{1/2}^\sigma 6d_{3/2}^\delta$ 31% $7s_{1/2}^\sigma 6d_{5/2}^\delta$
(2)2	13702	2.145	496	–	1.6	53% $(1)^1\Delta + 42\% (1)^3\Pi$	38% $7s_{1/2}^\sigma 6d_{5/2}^\delta$ 37% $7s_{1/2}^\sigma 6d_{3/2}^\delta$
(3)2	14600	2.142	509	–	1.5	56% $(1)^3\Pi + 43\% (1)^1\Delta$	51% $7s_{1/2}^\sigma 6d_{3/2}^\delta$ 22% $7s_{1/2}^\sigma 6d_{5/2}^\delta$
(4)2	21887	2.168	–	–	2.9	83% $(1)^3\Phi + 6\% (2)^3\Pi$	79% $6d_{3/2}^\delta 6d_{1/2}^\pi$ 11% $6d_{3/2}^\delta 7p_{1/2}^\pi$
(5)2	22248	2.115	–	–	1.0	92% $(2)^3\Pi + 6\% (1)^3\Phi$	80% $7s_{1/2}^\sigma 7p_{3/2}^\pi$
(6)2	25668	2.165	490	–	1.2	79% $(3)^3\Pi + 15\% (2)^3\Delta$	73% $6d_{5/2}^\delta 6d_{1/2}^\pi$
(7)2	27626	2.177	475	–	2.0	55% $(2)^3\Delta + 25\% (2)^1\Delta$	73% $6d_{1/2}^\pi 6d_{3/2}^\delta$
(8)2	29777	2.173	478	–	1.9	63% $(2)^1\Delta + 21\% (2)^3\Delta$	72% $6d_{5/2}^\delta 6d_{1/2}^\pi$
(9)2	31249	2.140	505	–	2.9	95% $(2)^3\Phi$	77% $6d_{3/2}^\delta 7p_{1/2}^\pi$ 12% $6d_{3/2}^\delta 6d_{1/2}^\pi$
(10)2	32413	2.180	463	–	1.9	84% $(3)^1\Delta + 7\% (5)^3\Pi$	55% $6d_{3/2}^\delta 6d_{1/2}^\pi$ 11% $6d_{3/2}^\delta 7p_{1/2}^\pi$
(11)2	34634	2.127	515	–	1.1	93% $(4)^3\Pi$	77% $6d_{5/2}^\delta 7p_{1/2}^\pi$
(1)3	10106	2.130	518	–	2.0	100% $(1)^3\Delta$	97% $7s_{1/2}^\sigma 6d_{5/2}^\delta$
(2)3	24020	2.167	481	–	2.9	91% $(1)^3\Phi + 8\% (2)^3\Delta$	51% $6d_{5/2}^\delta 6d_{1/2}^\pi$ 31% $6d_{3/2}^\delta 6d_{3/2}^\delta$
(3)3	27573	2.170	473	–	2.7	55% $(1)^1\Phi + 38\% (2)^3\Delta$	39% $6d_{3/2}^\delta 6d_{3/2}^\delta$ 25% $6d_{5/2}^\delta 6d_{1/2}^\pi$
(4)3	29633	2.169	483	–	2.5	53% $(2)^3\Delta + 44\% (1)^1\Phi$	59% $6d_{5/2}^\delta 6d_{1/2}^\pi$ 11% $6d_{5/2}^\delta 6d_{1/2}^\pi$
(5)3	32599	2.130	516	–	3.0	95% $(2)^3\Phi$	49% $6d_{3/2}^\delta 7p_{3/2}^\pi$ 28% $6d_{5/2}^\delta 7p_{1/2}^\pi$
(1)4	25259	2.156	485	–	3.8	76% $(1)^1\Gamma + 23\% (1)^3\Phi$	76% $6d_{5/2}^\delta 6d_{3/2}^\delta$ 14% $6d_{5/2}^\delta 6d_{3/2}^\delta$
(2)4	26612	2.159	495	–	3.2	76% $(1)^3\Phi + 24\% (1)^1\Gamma$	68% $6d_{5/2}^\delta 6d_{3/2}^\delta$ 15% $6d_{5/2}^\delta 6d_{3/2}^\delta$
(3)4	34159	2.122	525	–	3.0	99% $(2)^3\Phi$	77% $6d_{5/2}^\delta 7p_{3/2}^\pi$ 12% $6d_{5/2}^\delta 6d_{3/2}^\delta$



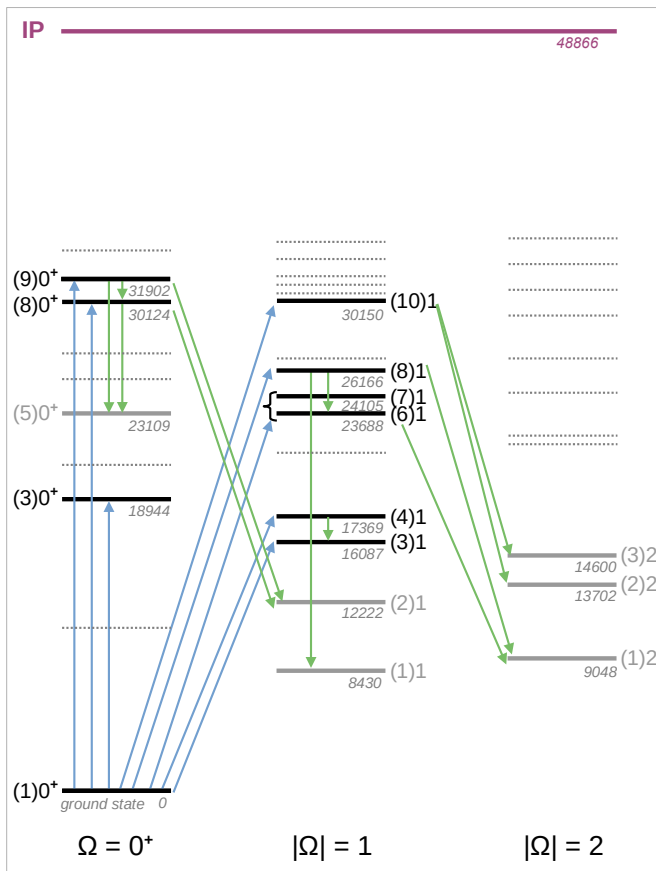


FIG. 3. The strongest transitions (blue arrows) from the  $X(1)0^+$  ground state of AcF and the strongest emissions for stimulated emission (green arrows). Levels accessible with two-step excitations are shown with solid grey lines. Dotted lines depict electronic states that are hardly accessible from the ground state with either direct or two-step excitations. It is noted that all transitions to the  $\Omega = 0^-$  states have low probabilities and are not shown here.  $T_e$  values ( $\text{cm}^{-1}$ ) are shown.

that, to obtain the full probability of such a two-step excitation process, these  $|d|^2$  values should be additionally multiplied by their counterparts from Tab. II. While the higher-lying states can thus be observed in principle, it is expected that due to the very complicated picture of excited states above  $35,000 \text{ cm}^{-1}$ , the experimentally measured vibrational progressions would be strongly perturbed and nearly uninformative.

In contrast, stimulated emission to lower-lying excited states seems to be much more promising for experimental studies of the electronic spectrum of AcF. Tables IV and V present radiative properties of several excited states with  $\Omega = 0^+$  and  $|\Omega| = 1$ , respectively. Based on these estimates, one can expect that at least four more excited states below  $32,000 \text{ cm}^{-1}$  can be accessed and studied via such a two-step approach. The  $(8)0^+$  and  $(9)0^+$  states can be used to repump AcF to the  $(5)0^+$  and  $(2)1$  states, while the  $(1)1$  and  $(1)2$  components of the

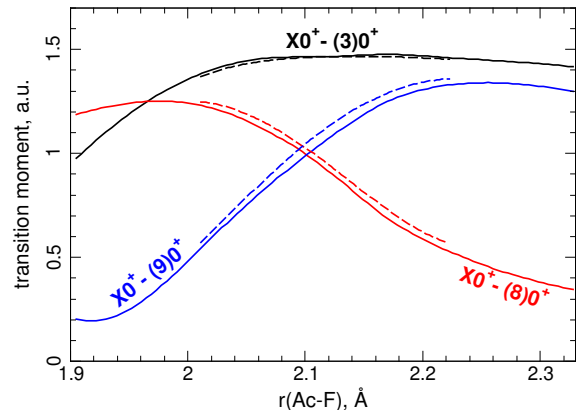


FIG. 4. Transition dipole moment functions for the most intense transitions from the  $X0^+$  ground state to excited states with  $\Omega = 0^+$ . Solid and dashed lines denote the direct [97] and finite-field [108] methods, respectively.

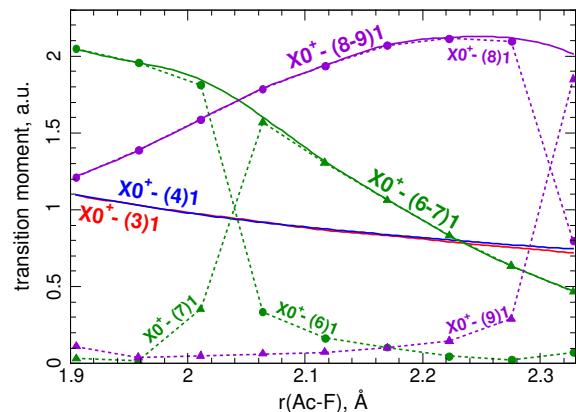


FIG. 5. Transition dipole moment (TDM) functions for the most intense transitions from the  $X0^+$  ground state to excited states with  $|\Omega| = 1$ . Abrupt changes in TDM functions are due to the presence of avoided crossings. For the  $(6)1 \sim (7)1$  and  $(8)1 \sim (9)1$  complexes, a transformation from adiabatic to spectroscopic “quasidiabatic” states was performed (see Refs. [110, 111] for details).

low-lying  $(1)^3\Delta$  triplet are accessible via the  $(8)1$  state. Note that the actual manifold of attainable electronic states is eventually determined by the capabilities of the experimental setup.

TABLE III. The most probable ( $|d|^2 > 0.5$ ) *vertical* transitions to *higher-lying* states with energies below 43,000  $\text{cm}^{-1}$  from the excited states that are easily accessible from the ground state. Energy levels and  $|d|^2$  values were calculated for  $r(\text{Ac-F}) = 4.0$  a.u. = 2.117 Å. † denotes states obtained as the intermediate ones in the IH-FS-RCC technique.

Initial state	$\rightarrow \Omega = 0^+$			$\rightarrow \Omega = 0^-$			$\rightarrow  \Omega  = 1$			$\rightarrow  \Omega  = 2$		
	state	$E, \text{cm}^{-1}$	$ d ^2, \text{a.u.}$	state	$E, \text{cm}^{-1}$	$ d ^2, \text{a.u.}$	state	$E, \text{cm}^{-1}$	$ d ^2, \text{a.u.}$	state	$E, \text{cm}^{-1}$	$ d ^2, \text{a.u.}$
(3)0 <sup>+</sup> → (19105 cm <sup>-1</sup> )	(4)0 <sup>+</sup>	20948	0.71				(16)1	36024	0.59			
	(15)0 <sup>+</sup>	37414	0.52				(26)1	39602	1.06			
	(17)0 <sup>+</sup>	39146	0.76				(32)1	42505	1.03			
(8)0 <sup>+</sup> → (30237 cm <sup>-1</sup> )	(9)0 <sup>+</sup>	31910	1.23				(17)1	36268	0.54			
	(10)0 <sup>+</sup>	33570	0.78				(20)1	37602	0.88			
	(11)0 <sup>+</sup>	33742	0.93									
	(17)0 <sup>+</sup>	39146	1.62									
(9)0 <sup>+</sup> → (31910 cm <sup>-1</sup> )	(10)0 <sup>+</sup>	33570	2.33				18(1)	36900	0.87			
	(11)0 <sup>+</sup>	33742	2.28				20(1)	37602	2.99			
	(17)0 <sup>+</sup>	39146	5.87				23(1)	38598	1.24			
	(18)0 <sup>+</sup>	40032	0.54									
(3)1→ (16239 cm <sup>-1</sup> )	(18)0 <sup>+</sup>	40032	1.08	(9)0 <sup>-</sup>	36136	0.75				(10)2	32652	0.98
				(12)0 <sup>-</sup>	38796	0.84				(15)2	38026	1.08
				(13)0 <sup>-</sup>	38823	1.14				(17)2	39131	0.60
				(15)0 <sup>-</sup>	40465 <sup>†</sup>	0.86				(18)2	40302	0.56
										(21)2	41759	0.57
(4)1→ (17531 cm <sup>-1</sup> )	(21)0 <sup>+</sup>	42460	0.65	(7)0 <sup>-</sup>	33399	0.80	(23)1	38598	0.59	(10)2	32652	0.52
				(8)0 <sup>-</sup>	34206	0.75				(17)2	39131	1.16
				(12)0 <sup>-</sup>	38796	1.88				(21)2	41759	1.32
				(14)0 <sup>-</sup>	39978	0.85				(23)2	42476	0.57
(7)1→ (24125 cm <sup>-1</sup> )	(11)0 <sup>+</sup>	33742	0.68	(6)0 <sup>-</sup>	32330	0.85				(13)2	37394	3.53
	(13)0 <sup>+</sup>	36395	0.62	(11)0 <sup>-</sup>	37776	0.53				(17)2	39131	1.20
	(15)0 <sup>+</sup>	37414	0.73	(12)0 <sup>-</sup>	38796	0.91						
				(13)0 <sup>-</sup>	38823	0.58						
(8)1→ (26171 cm <sup>-1</sup> )	(10)0 <sup>+</sup>	33570	1.16				(26)1	39602	0.69	(13)2	37394	2.12
	(11)0 <sup>+</sup>	33742	1.49							(18)2	39131	0.73
	(13)0 <sup>+</sup>	36395	1.39							(19)2	40302	0.96

TABLE IV. Squared transition dipole moments  $|d|^2$  for transitions to *lower-lying states* and radiative lifetimes  $\tau$  of several excited states with  $|\Omega| = 0^+$  of AcF accessible from the ground state.  $|d|^2$  values were calculated for  $r(\text{Ac-F}) = 4.0$  a.u. = 2.117 Å. Partial lifetimes for the channels with negligible contributions to the total decay rates are not shown.

$\rightarrow$	$(3)0^+ \rightarrow$		$(8)0^+ \rightarrow$		$(9)0^+ \rightarrow$	
	$ d ^2, \text{a.u.}$	$\tau$	$ d ^2, \text{a.u.}$	$\tau$	$ d ^2, \text{a.u.}$	$\tau$
(1)0 <sup>+</sup>	2.145	35.2 ns	0.862	34.8 ns	1.122	12.3 ns
(2)0 <sup>+</sup>	0.050	33.3 $\mu\text{s}$	0.097	736 ns	0.077	836 ns
(3)0 <sup>+</sup>			0.246	1.63 $\mu\text{s}$	0.077	2.34 $\mu\text{s}$
(4)0 <sup>+</sup>			0.001	624 $\mu\text{s}$	0.095	4.21 $\mu\text{s}$
(5)0 <sup>+</sup>			0.474	2.55 $\mu\text{s}$	0.433	1.85 $\mu\text{s}$
(6)0 <sup>+</sup>			0.000	44.9 ms	0.008	362 $\mu\text{s}$
(7)0 <sup>+</sup>			0.229	201 $\mu\text{s}$	0.066	72.6 $\mu\text{s}$
(8)0 <sup>+</sup>					1.234	83.0 $\mu\text{s}$
(1)1	0.062	8.89 $\mu\text{s}$	0.024	1.88 $\mu\text{s}$	0.007	5.63 $\mu\text{s}$
(2)1	0.001	672 $\mu\text{s}$	0.810	92.9 ns	0.752	98.5 ns
(3)1	0.029	999 $\mu\text{s}$	0.150	1.10 $\mu\text{s}$	0.008	17.8 $\mu\text{s}$
(4)1	0.011	16.5 ms	0.011	63.0 $\mu\text{s}$	0.109	1.59 $\mu\text{s}$
(5)1			0.335	1.94 $\mu\text{s}$	0.232	1.83 $\mu\text{s}$
(6-7)1			0.203	10.0 $\mu\text{s}$	0.037	38.1 $\mu\text{s}$
(8)1			0.301	40.1 $\mu\text{s}$	0.378	7.30 $\mu\text{s}$
(9)1			0.133	171 $\mu\text{s}$	0.047	168 $\mu\text{s}$
(10)1			0.131		0.001	
(11)1					0.016	
(12)1					0.000	
$\tau_{\text{total}}$		35.0 ns		22.8 ns		10.5 ns

### Suitability for direct laser cooling

The fact that the potential energy curves are to some extent parallel to each other indicates that a closed optical loop might exist, which would make AcF suitable for direct laser cooling. To achieve laser coolability, the upper electronic state must meet three basic conditions [122–124]: (a) a lifetime of order  $10^1 - 10^2$  ns, (b) a quasidiagonal Franck-Condon matrix, and (c) absence of decays to other electronic states (or quite small branching ratios less than  $10^{-3}$ ). It can be immediately seen from Tables IV and V that the last condition is definitely not fulfilled for the states  $(8)0^+$  (the largest branching ratio  $X0^+:(2)1$  equals to 1:0.38),  $(9)0^+$  (1:0.13),  $(3)1$  (1:0.02),  $(4)1$  (1:0.009) and  $(8)1$  (1:0.04).

The  $(3)0^+$  state also possesses quite large but not fully prohibitive branching ratios, the largest of which (1:0.005) is for the  $(3)0^+ \rightarrow (1)1$  decay channel. The sums for the first three (0.9876) and four (0.9980) Franck-Condon factors for the  $X0^+ - (3)0^+$  transition are not optical, but do not allow one to unequivocally reject the existence of a quasi-closed optical loop. Thus, experimental data on

TABLE V. Squared transition dipole moments  $|d|^2$  for transitions to *lower-lying states* and radiative lifetimes  $\tau$  of several excited states with  $|\Omega| = 1$  of AcF accessible from the ground state.  $|d|^2$  values were calculated for  $r(\text{Ac-F}) = 4.0$  a.u. = 2.117 Å. Partial lifetimes for the channels with negligible contributions to the total decay rates are not shown.

$\rightarrow$	$(3)1 \rightarrow$		$(4)1 \rightarrow$		$(8)1 \rightarrow$	
	$ d ^2, \text{a.u.}$	$\tau$	$ d ^2, \text{a.u.}$	$\tau$	$ d ^2, \text{a.u.}$	$\tau$
(1)0 <sup>+</sup>	0.752	178 ns	0.766	139 ns	3.751	7.14 ns
(2)0 <sup>+</sup>	0.071	77.0 $\mu\text{s}$	0.026	101 $\mu\text{s}$	0.003	48.5 $\mu\text{s}$
(3)0 <sup>+</sup>					0.160	8.15 $\mu\text{s}$
(4)0 <sup>+</sup>					0.012	301 $\mu\text{s}$
(5)0 <sup>+</sup>					0.099	211 $\mu\text{s}$
(1)0 <sup>-</sup>	0.072	57.3 $\mu\text{s}$	0.045	46.8 $\mu\text{s}$	0.004	40.3 $\mu\text{s}$
(2)0 <sup>-</sup>			0.011	237 ms	0.046	13.4 $\mu\text{s}$
(3)0 <sup>-</sup>					0.006	566 $\mu\text{s}$
(1)1	0.000	4.44 ms	0.004	188 $\mu\text{s}$	0.406	226 ns
(2)1	0.005	1.27 ms	0.088	39.1 $\mu\text{s}$	0.031	6.40 $\mu\text{s}$
(3)1			0.421	574 $\mu\text{s}$	0.022	17.8 $\mu\text{s}$
(4)1					0.152	4.70 $\mu\text{s}$
(5)1					0.049	92.9 $\mu\text{s}$
(6-7)1					0.615	93.7 $\mu\text{s}$
(1)2	0.158	9.66 $\mu\text{s}$	0.059	15.4 $\mu\text{s}$	0.552	195 ns
(2)2	0.002	1.44 ms	0.168	42.8 $\mu\text{s}$	0.007	37.7 $\mu\text{s}$
(3)2	0.086	946 $\mu\text{s}$	0.022	9.12 ms	0.022	6.85 $\mu\text{s}$
(4-5)2					0.007	478 $\mu\text{s}$
(6)2					0.003	
$\tau_{\text{total}}$		174 ns		136 ns		6.65 ns

the  $X0^+$  and  $(3)0^+$  states are necessary to resolve this question.

Finally we note that a closed loop employing some rovibronic state of the spin-orbit-coupled complex  $(6)1 \sim (7)1$  is also possible in principle, but a non-adiabatic model that combines theoretical and experimental data is needed to clarify this question.

### The $(1)^3\Delta$ state for $\mathcal{T}, \mathcal{P}$ -violation searches

The three lowest-lying excited states of AcF,  $(1)1$ ,  $(1)2$  and  $(1)3$  are components of the  $(1)^3\Delta$  triplet state split by the spin-orbit interaction. In the non-relativistic realm and the  $E1$  approximation, the  $(1)^3\Delta \rightarrow X^1\Sigma^+$  transitions are forbidden, but the spin-orbit interaction opens the transition from the  $^3\Delta_1 \equiv (1)1$  component to the ground state, making this state metastable. The same picture exists for the HfF<sup>+</sup> and ThO molecules [97, 116, 125–127], where the  $^3\Delta_1$  metastable states were used to place the most stringent upper bound on the electron electric dipole moment ( $e\text{EDM}$ ) to date [128, 129]. TDMs between the  $(1)^3\Delta_1$  and the ground electronic state and

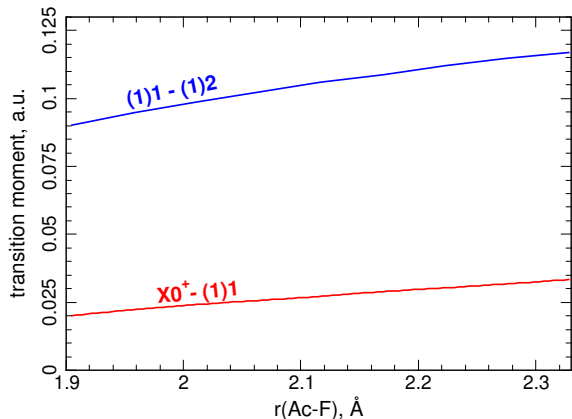


FIG. 6. Transition dipole moment functions for transitions from the  $(1)^3\Delta$  state components.

between the  $|\Omega| = 1$  and 2 components of  $(1)^3\Delta$  are presented in Fig. 6. For the  $(1)^3\Delta_1$  state, the sum rule [112] gives a lifetime of 1.07 ms, which is approximately 4 times less than for ThO (4.2(0.5) ms [130]) and 2000 times less than for  $\text{HfF}^+$  (2.1(0.2) s [131]). Thus, a shorter coherence time can be achieved with AcF than with systems currently used in  $e\text{EDM}$  experiments.

The lifetime of the  $(1)^3\Delta_2$  state is predicted to be 181 ms (cf.  $> 62$  ms for ThO [132]). In principle, this electronic state could also be used to measure  $\mathcal{T}, \mathcal{P}$ -violating properties, such as the  $e\text{EDM}$ . However, the effective electric field acting on the  $e\text{EDM}$  in the  $^3\Delta_2$  state is expected to be smaller than that for the  $^3\Delta_1$  state. Additionally, the electronic  $g$ -factor in the  $^3\Delta_2$  state is much larger than in the  $^3\Delta_1$  state, where it is zero in the non-relativistic approximation and thus allows for a significant reduction of systematic effects associated with stray magnetic fields.

### The ground state for searches of nuclear properties

The electronic ground state  $X^1\Sigma^+ \equiv X0^+$  of AcF can be used to search for the  $\mathcal{T}, \mathcal{P}$ -violating nuclear Schiff moment [39, 40]. The use of the ground state in such experiments implies that the coherence time is not limited by the lifetime of the working state. Moreover, other  $\mathcal{T}, \mathcal{P}$ -violating effects, e.g. those induced by the nuclear magnetic quadrupole moment, are strongly suppressed as they appear in the first order only for paramagnetic systems. Consequently, the interpretation of an experiment to measure the nuclear Schiff moment would be more direct.

Another possible use of the electronic ground state of AcF is the measurement of the Ac nuclear electric

quadrupole moment. As it was demonstrated above, a highly accurate theoretical description of this state is tractable, and high-order coupled cluster methods are possible. Consequently, the electric field gradient at the Ac nucleus can be calculated with a very high accuracy. Therefore, a high-precision measurement of the molecular hyperfine structure can be used to extract the electric quadrupole moment of the actinium nucleus with high precision and accuracy.

## CONCLUSION

In the present work, the first comprehensive theoretical study of the electronic structure of AcF, with term energies below  $35,000 \text{ cm}^{-1}$  and their radiative properties, is reported. We confirm the ground state to be a closed-shell singlet, and thus sensitive to the nuclear Schiff moment, and the  $\text{IP}_e$  is calculated to be  $48,866(130) \text{ cm}^{-1}$ . The obtained value for the dissociation energy is  $D_e = 57,214(234) \text{ cm}^{-1}$ . The strongest transitions from the ground state are identified theoretically and can be used for experimental studies at the CRIS experiment at ISOLDE. Possible two-excitation pathways to excited electronic states below  $43,000 \text{ cm}^{-1}$  that are not directly accessible from the ground one are proposed. Preliminary estimates based on calculated branching ratios and Franck-Condon factors allow one to assert that the molecule is not an ideal candidate for direct laser cooling, but experimental data on the  $X0^+$  and  $(3)0^+$  states are needed to unambiguously resolve the suitability. The lifetime of the metastable  $(1)^3\Delta_1$  state, which can be used to search for the  $\mathcal{T}, \mathcal{P}$ -violating electric dipole moment of the electron is, estimated to be 1.07 ms.

## ACKNOWLEDGEMENTS

We are grateful to Anatoly V. Titov for useful discussions. Electronic structure calculations have been carried out using computing resources of the federal collective usage center Complex for Simulation and Data Processing for Mega-science Facilities at National Research Centre “Kurchatov Institute”, <http://ckp.nrcki.ru/>.

The computational study of AcF excited states and transition moments performed at NRC “Kurchatov Institute” – PNPI by AVO, AZ and NSM was supported by the Russian Science Foundation (Grant No. 20-13-00225-P, <https://rscf.ru/en/project/23-13-45028/>). AcF ionization potential and dissociation energy calculations performed at NRC “Kurchatov Institute” – PNPI by LVS were supported by the Russian Science Foundation Grant No. 19-72-10019-P (<https://rscf.ru/en/project/22-72-41010/>). GN and MAK acknowledge support from the Belgian Excellence of Science project No. 40007501



(MANASLU) and the Flemish Science Foundation (FWO). MAU acknowledges support from the EU Horizon 2020 Research and Innovation Program No. 861198 (LISA) Marie Skłodowska-Curie Innovative Training Network (ITN).

\* skripnikov\_lv@pnpi.nrcki.ru,  
leonidos239@gmail.com

† oleynichenko\_av@pnpi.nrcki.ru,  
alexvoleyichenko@gmail.com

- [1] G. Arrowsmith-Kron, M. Athanasakis-Kaklamanakis, M. Au, J. Ballof, R. Berger, A. Borschevsky, A. A. Breier, F. Buchinger, D. Budker, L. Caldwell, C. Charles, N. Dattani, R. P. de Groote, D. DeMille, T. Dickel, J. Dobaczewski, C. E. Düllmann, E. Eliav, J. Engel, M. Fan, V. Flambaum, K. T. Flanagan, A. Gaiser, R. Garcia Ruiz, K. Gaul, T. F. Giesen, J. Ginges, A. Gottberg, G. Gwinner, R. Heinke, S. Hoekstra, J. D. Holt, N. R. Hutzler, A. Jayich, J. Karthein, K. G. Leach, K. Madison, S. Malbrunot-Ettenauer, T. Miyagi, I. D. Moore, S. Moroch, P. Navrátil, W. Nazarewicz, G. Neyens, E. Norrgard, N. Nussgart, L. F. Pašteka, A. N. Petrov, W. Plass, R. A. Ready, M. P. Reiter, M. Reponen, S. Rothe, M. Safronova, C. Scheidenberger, A. Shindler, J. T. Singh, L. V. Skripnikov, A. V. Titov, S.-M. Udrescu, S. G. Wilkins, and X. Yang, Opportunities for fundamental physics research with radioactive molecules (2023), [arXiv:arXiv:2302.02165](https://arxiv.org/abs/2302.02165) [nucl-ex].
- [2] J. S. M. Ginges and V. V. Flambaum, Violations of fundamental symmetries in atoms and tests of unification theories of elementary particles, *Phys. Rep.* **397**, 63 (2004).
- [3] P. W. Graham and S. Rajendran, New observables for direct detection of axion dark matter, *Phys. Rev. D* **88**, 035023 (2013).
- [4] B. M. Roberts, V. A. Dzuba, and V. V. Flambaum, Parity and time-reversal violation in atomic systems, *Annu. Rev. Nucl. Part. Sci.* **65**, 63 (2015).
- [5] M. S. Safronova, D. Budker, D. DeMille, D. F. J. Kimball, A. Derevianko, and C. W. Clark, Search for new physics with atoms and molecules, *Rev. Mod. Phys.* **90**, 025008 (2018).
- [6] R. Alarcon, J. Alexander, V. Anastassopoulos, T. Aoki, R. Baartman, S. Baessler, L. Bartoszek, D. H. Beck, F. Bedeschi, R. Berger, M. Berz, H. L. Bethlem, T. Bhattacharya, M. Blaskiewicz, T. Blum, T. Bowcock, A. Borschevsky, K. Brown, D. Budker, S. Burdin, B. C. Casey, G. Casse, G. Cantatore, L. Cheng, T. Chupp, V. Cianciolo, V. Cirigliano, S. M. Clayton, C. Crawford, B. P. Das, H. Davoudiasl, J. de Vries, D. DeMille, D. Denisov, M. V. Diwan, J. M. Doyle, J. Engel, G. Fanourakis, R. Fatemi, B. W. Filippone, V. V. Flambaum, T. Fleig, N. Fomin, W. Fischer, G. Gabrielse, R. F. Garcia Ruiz, A. Gardikiotis, C. Gatti, A. Geraci, J. Gooding, B. Golub, P. Graham, F. Gray, W. C. Griffith, S. Haciomeroglu, G. Gwinner, S. Hoekstra, G. H. Hoffstaetter, H. Huang, N. R. Hutzler, M. Incagli, T. M. Ito, T. Izubuchi, A. M. Jayich, H. Jeong, D. Kaplan, M. Karuza, D. Kawall, O. Kim, I. Koop, W. Korsch, E. Korobkina, V. Lebedev, J. Lee, S. Lee, R. Lehnert, K. K. H. Leung, C.-Y. Liu, J. Long, A. Lusiani, W. J. Marciano, M. Maroudas, A. Matlashov, N. Matsumoto, R. Mawhorter, F. Meot, E. Mereghetti, J. P. Miller, W. M. Morse, J. Mott, Z. Omarov, L. A. Orozco, C. M. O’Shaughnessy, C. Ozben, S. Park, R. W. Pattie Jr., A. N. Petrov, G. M. Piacentino, B. R. Plaster, B. Podobedov, M. Poelker, D. Pocanic, V. S. Prasanna, J. Price, M. J. Ramsey-Musolf, D. Raparia, S. Rajendran, M. Reece, A. Reid, S. Rescia, A. Ritz, B. L. Roberts, M. S. Safronova, Y. Sakemi, P. Schmidt-Wellenburg, A. Shindler, Y. K. Semertzidis, A. Silenko, J. T. Singh, L. V. Skripnikov, A. Soni, E. Stephenson, R. Suleiman, A. Sunaga, M. Syphers, S. Syritsyn, M. R. Tarbutt, P. Thoerngren, R. G. E. Timmermans, V. Tishchenko, A. V. Titov, N. Tsoupas, S. Tzamarias, A. Variola, G. Venanzoni, E. Vilella, J. Vossebel, P. Winter, E. Won, A. Zelenski, T. Zelevinsky, Y. Zhou, and K. Zioutas, Electric dipole moments and the search for new physics (2022), [arXiv:arXiv:2203.08103](https://arxiv.org/abs/2203.08103) [hep-ph].
- [7] I. B. Khriplovich, *Parity non-conservation in atomic phenomena* (Gordon and Breach, New York, 1991).
- [8] I. B. Khriplovich and S. K. Lamoreaux, *CP Violation without Strangeness. The Electric Dipole Moments of Particles, Atoms, and Molecules* (Springer-Verlag, Berlin, 1997).
- [9] M. Kozlov and L. Labzowsky, Parity violation effects in diatomics, *J. Phys. B* **28**, 1933 (1995).
- [10] T. A. Isaev, S. Hoekstra, and R. Berger, Laser-cooled RaF as a promising candidate to measure molecular parity violation, *Phys. Rev. A* **82**, 052521 (2010).
- [11] T. A. Isaev, A. V. Zaitsevskii, and E. Eliav, Laser-coolable polyatomic molecules with heavy nuclei, *J. Phys. B: At. Mol. Opt. Phys.* **50**, 225101 (2017).
- [12] I. Kozyryev and N. R. Hutzler, Precision measurement of time-reversal symmetry violation with laser-cooled polyatomic molecules, *Phys. Rev. Lett.* **119**, 133002 (2017).
- [13] J. Lim, J. R. Almond, M. A. Trigatzis, J. A. Devlin, N. J. Fitch, B. E. Sauer, M. R. Tarbutt, and E. A. Hinds, Laser cooled YbF molecules for measuring the electron’s electric dipole moment, *Phys. Rev. Lett.* **120**, 123201 (2018).
- [14] Y. Hao, L. F. Pašteka, L. Visscher, P. Aggarwal, H. L. Bethlem, A. Boeschoten, A. Borschevsky, M. Denis, K. Esajas, S. Hoekstra, K. Jungmann, V. R. Marshall, T. B. Meijknecht, M. C. Mooij, R. G. E. Timmermans, A. Touwen, W. Ubachs, L. Willmann, Y. Yin, and A. Zapara, High accuracy theoretical investigations of CaF, SrF, and BaF and implications for laser-cooling, *J. Chem. Phys.* **151**, 034302 (2019).
- [15] B. L. Augenbraun, Z. D. Lasner, A. Frenett, H. Sawaoka, C. Miller, T. C. Steimle, and J. M. Doyle, Laser-cooled polyatomic molecules for improved electron electric dipole moment searches, *New J. Phys.* **22**, 022003 (2020).
- [16] A. V. Oleynichenko, L. V. Skripnikov, A. V. Zaitsevskii, and V. V. Flambaum, Laser-coolable AcOH<sup>+</sup> ion for CP-violation searches, *Phys. Rev. A* **105**, 022825 (2022).
- [17] B. L. Augenbraun, Z. D. Lasner, A. Frenett, H. Sawaoka, A. T. Le, J. M. Doyle, and T. C. Steimle, Observation and laser spectroscopy of ytterbium monomethoxide, YbOCH<sub>3</sub>, *Phys. Rev. A* **103**,

- 022814 (2021).
- [18] C. Zülch, K. Gaul, S. M. Giesen, R. F. Garcia Ruiz, and R. Berger, Cool molecular highly charged ions for precision tests of fundamental physics (2022), [arXiv:arXiv:2203.10333](https://arxiv.org/abs/2203.10333) [physics.chem-ph].
- [19] T. Isaev, D. Makinskii, and A. Zaitsevskii, Radium-containing molecular cations amenable for laser cooling, *Chem. Phys. Lett.* **807**, 140078 (2022).
- [20] N. Auerbach, V. V. Flambaum, and V. Spevak, Collective  $T$ - and  $P$ -odd electromagnetic moments in nuclei with octupole deformations, *Phys. Rev. Lett.* **76**, 4316 (1996).
- [21] J. Dobaczewski and J. Engel, Nuclear time-reversal violation and the Schiff moment of  $^{225}\text{Ra}$ , *Phys. Rev. Lett.* **94**, 232502 (2005).
- [22] N. Auerbach, V. F. Dmitriev, V. V. Flambaum, A. Lisetskiy, R. A. Sen'kov, and V. G. Zelevinsky, Nuclear Schiff moment in nuclei with soft octupole and quadrupole vibrations, *Phys. Rev. C* **74**, 025502 (2006).
- [23] P. A. Butler, Pear-shaped atomic nuclei, *Proc. Math. Phys. Eng. Sci.* **476**, 20200202 (2020).
- [24] V. V. Flambaum and H. Feldmeier, Enhanced nuclear Schiff moment in stable and metastable nuclei, *Phys. Rev. C* **101**, 015502 (2020).
- [25] V. V. Flambaum and A. J. Mansour, Enhanced magnetic quadrupole moments in nuclei with octupole deformation and their  $cp$ -violating effects in molecules, *Phys. Rev. C* **105**, 065503 (2022).
- [26] A. D. Sakharov, Violation of CP Invariance, C Asymmetry, and Baryon Asymmetry of the Universe, *JETP Lett.* **5**, 27 (1967).
- [27] M. Dine and A. Kusenko, Origin of the matter-antimatter asymmetry, *Rev. Mod. Phys.* **76**, 1 (2003).
- [28] M. V. Romalis, W. C. Griffith, J. P. Jacobs, and E. N. Fortson, New limit on the permanent electric dipole moment of  $^{199}\text{Hg}$ , *Phys. Rev. Lett.* **86**, 2505 (2001).
- [29] W. C. Griffith, M. D. Swallows, T. H. Loftus, M. V. Romalis, B. R. Heckel, and E. N. Fortson, Improved limit on the permanent electric dipole moment of  $^{199}\text{Hg}$ , *Phys. Rev. Lett.* **102**, 101601 (2009).
- [30] B. Graner, Y. Chen, E. G. Lindahl, and B. R. Heckel, Reduced limit on the permanent electric dipole moment of  $^{199}\text{Hg}$ , *Phys. Rev. Lett.* **116**, 161601 (2016).
- [31] M. A. Rosenberry and T. E. Chupp, Atomic electric dipole moment measurement using spin exchange pumped masers of  $^{129}\text{Xe}$  and  $^3\text{He}$ , *Phys. Rev. Lett.* **86**, 22 (2001).
- [32] N. Sachdeva, I. Fan, E. Babcock, M. Burghoff, T. E. Chupp, S. Degenkolb, P. Fierlinger, S. Haude, E. Kraegeloh, W. Kilian, S. Knappe-Grüneberg, F. Kuchler, T. Liu, M. Marino, J. Meinel, K. Rolfs, Z. Salhi, A. Schnabel, J. T. Singh, S. Stuiber, W. A. Terrano, L. Trahms, and J. Voigt, New limit on the permanent electric dipole moment of  $^{129}\text{Xe}$  using  $^3\text{He}$  comagnetometry and SQUID detection, *Phys. Rev. Lett.* **123**, 143003 (2019).
- [33] F. Allmendinger, I. Engin, W. Heil, S. Karpuk, H.-J. Krause, B. Niederländer, A. Offenhäusser, M. Repetto, U. Schmidt, and S. Zimmer, Measurement of the permanent electric dipole moment of the  $^{129}\text{Xe}$  atom, *Phys. Rev. A* **100**, 022505 (2019).
- [34] D. Cho, K. Sangster, and E. A. Hinds, Search for time-reversal-symmetry violation in thallium fluoride using a jet source, *Phys. Rev. A* **44**, 2783 (1991).
- [35] E. B. Norrgard, E. R. Edwards, D. J. McCarron, M. H. Steinecker, D. DeMille, S. S. Alam, S. K. Peck, N. S. Wadia, and L. R. Hunter, Hyperfine structure of the  $B^3\Pi_1$  state and predictions of optical cycling behavior in the  $X \rightarrow B$  transition of TIF, *Phys. Rev. A* **95**, 062506 (2017).
- [36] O. Grasdijk, O. Timgren, J. Kastelic, T. Wright, S. Lamoreaux, D. DeMille, K. Wenz, M. Aitken, T. Zelevinsky, T. Winick, and D. Kowall, CeNTREX: a new search for time-reversal symmetry violation in the  $^{205}\text{Tl}$  nucleus, *Quantum Sci. Technol.* **6**, 044007 (2021).
- [37] L. V. Skripnikov and A. V. Titov, Lcao-based theoretical study of  $\text{PbTiO}_3$  crystal to search for parity and time reversal violating interaction in solids, *J. Chem. Phys.* **145**, 054115 (2016).
- [38] D. Aybas, J. Adam, E. Blumenthal, A. V. Gramolin, D. Johnson, A. Kleyheeg, S. Afach, J. W. Blanchard, G. P. Centers, A. Garcon, M. Engler, N. L. Figueroa, M. G. Sendra, A. Wickenbrock, M. Lawson, T. Wang, T. Wu, H. Luo, H. Mani, P. Mauskopf, P. W. Graham, S. Rajendran, D. F. J. Kimball, D. Budker, and A. O. Sushkov, Search for axionlike dark matter using solid-state nuclear magnetic resonance, *Phys. Rev. Lett.* **126**, 141802 (2021).
- [39] V. V. Flambaum and V. A. Dzuba, Electric dipole moments of atoms and molecules produced by enhanced nuclear Schiff moments, *Phys. Rev. A* **101**, 042504 (2020).
- [40] L. V. Skripnikov, N. S. Mosyagin, A. V. Titov, and V. V. Flambaum, Actinide and lanthanide molecules to search for strong CP-violation, *Phys. Chem. Chem. Phys.* **22**, 18374 (2020).
- [41] E. Verstraelen, A. Teigelhöfer, W. Ryssens, F. Ames, A. Barzakh, M. Bender, R. Ferrer, S. Goriely, P.-H. Heenen, M. Huyse, P. Kunz, J. Lassen, V. Manea, S. Raeder, and P. Van Duppen, Search for octupole-deformed actinium isotopes using resonance ionization spectroscopy, *Phys. Rev. C* **100**, 044321 (2019).
- [42] F. Dalton, V. V. Flambaum, and A. J. Mansour, Enhanced Schiff and magnetic quadrupole moments in deformed nuclei and their connection to the search for axion dark matter, *Phys. Rev. C* **107**, 035502 (2023).
- [43] A. Morgenstern, C. Apostolidis, and F. Bruchertseifer, Supply and clinical application of actinium-225 and bismuth-213, *Semin. Nucl. Med.* **50**, 119 (2020).
- [44] R. Catherall, W. Andreatza, M. Breitenfeldt, A. Dorival, G. J. Focker, T. P. Gharsa, T. J. Giles, J. L. Grenard, F. Locci, P. Martins, S. Marzari, J. Schipper, A. Shornikov, and T. Stora, The ISOLDE facility, *J. Phys. G. Nucl. Part. Phys.* **44**, 1 (2017).
- [45] M. Au, M. Athanasakis-Kaklamanakis, L. Nies, J. Ballof, R. Berger, K. Chrysalidis, P. Fischer, R. Heinke, J. Johnson, U. Köster, D. Leimbach, B. Marsh, M. Mougeot, J. Reilly, E. Reis, M. Schlaich, C. Schweiger, L. Schweikhard, S. Stegemann, J. Wessolek, F. Wienholtz, S. G. Wilkins, W. Wojtaczka, C. E. Dillmann, and S. Rothe, In-source and in-trap formation of molecular ions in the actinide mass range at CERN-ISOLDE (2023), [arXiv:2303.12215](https://arxiv.org/abs/2303.12215) [physics.ins-det].
- [46] R. F. Garcia Ruiz, R. Berger, J. Billowes, C. L. Binnersley, M. L. Bissell, A. A. Breier, A. J. Brinson, K. Chrysalidis, T. E. Cocolios, B. S. Cooper, K. T. Flanagan, T. F. Giesen, R. P. de Groote, S. Franchoo, F. P. Gustafsson,

- T. A. Isaev, Á. Koszorus, G. Neyens, H. A. Perrett, C. M. Ricketts, S. Rothe, L. Schweikhard, A. R. Vernon, K. D. A. Wendt, F. Wienholtz, S. G. Wilkins, and X. F. Yang, Spectroscopy of short-lived radioactive molecules, *Nature* **581**, 396 (2020).
- [47] S. M. Udrescu, A. J. Brinson, R. F. Garcia Ruiz, K. Gaul, R. Berger, J. Billowes, C. L. Binnersley, M. L. Bissell, A. A. Breier, K. Chrysalidis, T. E. Cocolios, B. S. Cooper, K. T. Flanagan, T. F. Giesen, R. P. de Groote, S. Franchoo, F. P. Gustafsson, T. A. Isaev, Á. Koszorus, G. Neyens, H. A. Perrett, C. M. Ricketts, S. Rothe, A. R. Vernon, K. D. A. Wendt, F. Wienholtz, S. G. Wilkins, and X. F. Yang, Isotope shifts of radium monofluoride molecules, *Phys. Rev. Lett.* **127**, 033001 (2021).
- [48] S. M. Udrescu, S. G. Wilkins, A. A. Breier, R. F. Garcia Ruiz, M. Athanasakis-Kaklamanakis, M. Au, I. Belošević, R. Berger, M. L. Bissell, K. Chrysalidis, T. E. Cocolios, R. P. de Groote, A. Dorne, K. T. Flanagan, S. Franchoo, K. Gaul, S. Geldhof, T. F. Giesen, D. Hanstorp, R. Heinke, A. Koszorus, S. Kujanpää, L. Lalanne, G. Neyens, M. Nichols, H. A. Perrett, J. R. Reilly, S. Rothe, B. van den Borne, Q. Wang, J. Wessolek, X. F. Yang, and C. Zülch, Precision spectroscopy and laser cooling scheme of a radium-containing molecule, PREPRINT (Version 1) available at Research Square [<https://doi.org/10.21203/rs.3.rs-2648482/v1>] (2023).
- [49] T. Cocolios, R. de Groote, J. Billowes, M. Bissell, I. Budincevic, T. Day Goodacre, G. Farooq-Smith, V. Fedosseev, K. Flanagan, S. Franchoo, R. Garcia Ruiz, W. Gins, H. Heylen, T. Kron, R. Li, K. Lynch, B. Marsh, G. Neyens, R. Rossel, S. Rothe, A. Smith, H. Stroke, K. Wendt, S. Wilkins, and X. Yang, High-resolution laser spectroscopy with the collinear resonance ionisation spectroscopy (cris) experiment at cern-isolde, *Nucl. Instrum. Methods Phys. Res. B* **376**, 284 (2016), proceedings of the XVIIth International Conference on Electromagnetic Isotope Separators and Related Topics (EMIS2015), Grand Rapids, MI, U.S.A., 11-15 May 2015.
- [50] A. Vernon, R. de Groote, J. Billowes, C. Binnersley, T. Cocolios, G. Farooq-Smith, K. Flanagan, R. Garcia Ruiz, W. Gins, A. Koszorus, G. Neyens, C. Ricketts, A. Smith, S. Wilkins, and X. Yang, Optimising the collinear resonance ionisation spectroscopy (cris) experiment at cern-isolde, *Nuclear Instruments and Methods in Physics Research Section B: Beam Interactions with Materials and Atoms* **463**, 384 (2020).
- [51] Laser ionization spectroscopy of AcF (Proposal to the ISOLDE and Neutron Time-of-Flight Committee) (2021).
- [52] L. R. Hunter, S. K. Peck, A. S. Greenspon, S. Saad Alam, and D. DeMille, Prospects for laser cooling TlF, *Phys. Rev. A* **85**, 012511 (2012).
- [53] L. Visscher, T. J. Lee, and K. G. Dyall, Formulation and implementation of a relativistic unrestricted coupled-cluster method including noniterative connected triples, *J. Chem. Phys.* **105**, 8769 (1996).
- [54] R. J. Bartlett and M. Musiał, Coupled-cluster theory in quantum chemistry, *Rev. Mod. Phys.* **79**, 291 (2007).
- [55] K. Raghavachari, G. W. Trucks, J. A. Pople, and M. Head-Gordon, A fifth-order perturbation comparison of electron correlation theories, *Chem. Phys. Lett.* **157**, 479 (1989).
- [56] J. Noga, R. J. Bartlett, and M. Urban, Towards a full CCSDT model for electron correlation. CCSDT-n models, *Chem. Phys. Lett.* **134**, 126 (1987).
- [57] J. Noga and R. J. Bartlett, The full CCSDT model for molecular electronic structure, *J. Chem. Phys.* **86**, 7041 (1987).
- [58] Y. J. Bomble, J. F. Stanton, M. Kállay, and J. Gauss, Coupled-cluster methods including noniterative corrections for quadruple excitations, *J. Chem. Phys.* **123**, 054101 (2005).
- [59] M. Kállay and J. Gauss, Approximate treatment of higher excitations in coupled-cluster theory, *J. Chem. Phys.* **123**, 214105 (2005).
- [60] K. G. Dyall, Relativistic double-zeta, triple-zeta, and quadruple-zeta basis sets for the actinides Ac–Lr, *Theor. Chem. Acc.* **117**, 491 (2007).
- [61] K. G. Dyall, Core correlating basis functions for elements 31–118, *Theor. Chem. Acc.* **131**, 1217 (2012).
- [62] K. G. Dyall, Relativistic double-zeta, triple-zeta, and quadruple-zeta basis sets for the 5d elements Hf–Hg, *Theor. Chem. Acc.* **112**, 403 (2004).
- [63] K. G. Dyall and A. S. Gomes, Revised relativistic basis sets for the 5d elements Hf–Hg, *Theor. Chem. Acc.* **125**, 97 (2010).
- [64] K. G. Dyall, Relativistic double-zeta, triple-zeta, and quadruple-zeta basis sets for the light elements H–Ar, *Theor. Chem. Acc.* **135**, 128 (2016).
- [65] A. V. Titov and N. S. Mosyagin, Generalized relativistic effective core potential: Theoretical grounds, *Int. J. Quantum Chem.* **71**, 359 (1999).
- [66] N. S. Mosyagin, A. V. Zaitsevskii, and A. V. Titov, Shape-consistent relativistic effective potentials of small atomic cores, *Int. Rev. At. Mol. Phys* **1**, 63 (2010).
- [67] N. S. Mosyagin, A. V. Zaitsevskii, L. V. Skripnikov, and A. V. Titov, Generalized relativistic effective core potentials for actinides, *Int. J. Quantum Chem.* **116**, 301 (2016).
- [68] N. S. Mosyagin, Generalized relativistic effective core potentials for lanthanides, *Nonlinear Phenomena in Complex Systems* **20**, 111 (2017).
- [69] L. V. Skripnikov, Nuclear magnetization distribution effect in molecules: Ra<sup>+</sup> and RaF hyperfine structure, *J. Chem. Phys.* **153**, 114114 (2020).
- [70] L. V. Skripnikov, N. S. Mosyagin, and A. V. Titov, Relativistic coupled-cluster calculations of spectroscopic and chemical properties for element 120, *Chem. Phys. Lett.* **555**, 79 (2013).
- [71] T. H. Dunning, Jr, Gaussian basis sets for use in correlated molecular calculations. I. The atoms boron through neon and hydrogen, *J. Chem. Phys.* **90**, 1007 (1989).
- [72] R. A. Kendall, T. H. Dunning, Jr, and R. J. Harrison, Electron affinities of the first-row atoms revisited. Systematic basis sets and wave functions, *J. Chem. Phys.* **96**, 6796 (1992).
- [73] W. A. de Jong, R. J. Harrison, and D. A. Dixon, Parallel Douglas–Kroll energy and gradients in NWChem: Estimating scalar relativistic effects using Douglas–Kroll contracted basis sets, *J. Chem. Phys.* **114**, 48 (2001).
- [74] D. Feller and K. A. Peterson, Re-examination of atomization energies for the Gaussian-2 set of molecules, *J. Chem. Phys.* **110**, 8384 (1999).
- [75] J. Sikkema, L. Visscher, T. Saue, and M. Iliaš, The

- molecular mean-field approach for correlated relativistic calculations, *J. Chem. Phys.* **131**, 124116 (2009).
- [76] V. M. Shabaev, I. I. Tupitsyn, and V. A. Yerokhin, Model operator approach to the Lamb shift calculations in relativistic many-electron atoms, *Phys. Rev. A* **88**, 012513 (2013).
- [77] A. V. Malyshev, D. A. Glazov, V. M. Shabaev, I. I. Tupitsyn, V. A. Yerokhin, and V. A. Zaytsev, Model-qed operator for superheavy elements, *Phys. Rev. A* **106**, 012806 (2022).
- [78] L. V. Skripnikov, Approaching meV level for transition energies in the radium monofluoride molecule RaF and radium cation  $\text{Ra}^+$  by including quantum-electrodynamics effects, *J. Chem. Phys.* **154**, 201101 (2021).
- [79] DIRAC, a relativistic ab initio electronic structure program, Release DIRAC19 (2019), written by A. S. P. Gomes, T. Saue, L. Visscher, H. J. Aa. Jensen, and R. Bast, with contributions from I. A. Aucar, V. Bakken, K. G. Dyall, S. Dubillard, U. Ekstroem, E. Eliav, T. Enevoldsen, E. Fasshauer, T. Fleig, O. Fossgaard, L. Halbert, E. D. Hedegaard, T. Helgaker, J. Henriksson, M. Ilias, Ch. R. Jacob, S. Knecht, S. Komorovsky, O. Kullie, J. K. Laerdahl, C. V. Larsen, Y. S. Lee, H. S. Nataraj, M. K. Nayak, P. Norman, M. Olejniczak, J. Olsen, J. M. H. Olsen, Y. C. Park, J. K. Pedersen, M. Pernpointner, R. Di Remigio, K. Ruud, P. Salek, B. Schimmelpfennig, B. Senjean, A. Shee, J. Sikkema, A. J. Thorvaldsen, J. Thyssen, J. van Stralen, M. L. Vidal, S. Villaume, O. Visser, T. Winther, and S. Yamamoto (see <http://diracprogram.org>). (accessed on 14 April 2023).
- [80] T. Saue, R. Bast, A. S. P. Gomes, H. J. A. Jensen, L. Visscher, I. A. Aucar, R. Di Remigio, K. G. Dyall, E. Eliav, E. Fasshauer, T. Fleig, L. Halbert, E. D. Hedegård, B. Helmich-Paris, M. Iliáš, C. R. Jacob, S. Knecht, J. K. Laerdahl, M. L. Vidal, M. K. Nayak, M. Olejniczak, J. M. H. Olsen, M. Pernpointner, B. Senjean, A. Shee, A. Sunaga, and J. N. P. van Stralen, The DIRAC code for relativistic molecular calculations, *J. Chem. Phys.* **152**, 204104 (2020).
- [81] MRCC, MRCC, a quantum chemical program suite written by M. Kállay, P. R. Nagy, D. Mester, Z. Rolik, G. Samu, J. Csontos, J. Csóka, P. B. Szabó, L. Gyevi-Nagy, B. Hégyely, I. Ladjánszki, L. Szegedy, B. Ladóczki, K. Petrov, M. Farkas, P. D. Mezei, and Á. Ganyczec. See [www.mrcc.hu](http://www.mrcc.hu).
- [82] M. Kállay, P. R. Nagy, D. Mester, Z. Rolik, G. Samu, J. Csontos, J. Csóka, P. B. Szabó, L. Gyevi-Nagy, B. Hégyely, I. Ladjánszki, L. Szegedy, B. Ladóczki, K. Petrov, M. Farkas, P. D. Mezei, and Á. Ganyczec, The MRCC program system: Accurate quantum chemistry from water to proteins, *J. Chem. Phys.* **152**, 074107 (2020).
- [83] M. Kállay and P. R. Surján, Higher excitations in coupled-cluster theory, *J. Chem. Phys.* **115**, 2945 (2001).
- [84] M. Kállay, P. G. Szalay, and P. R. Surján, A general state-selective multireference coupled-cluster algorithm, *J. Chem. Phys.* **117**, 980 (2002).
- [85] J. F. Stanton, J. Gauss, M. E. Harding, P. G. Szalay, *et al.*, “CFour” (2011), CFour: a program package for performing high-level quantum chemical calculations on atoms and molecules, <http://www.cfour.de>.
- [86] D. A. Matthews, L. Cheng, M. E. Harding, F. Lipparini, S. Stopkowicz, T.-C. Jagau, P. G. Szalay, J. Gauss, and J. F. Stanton, Coupled-cluster techniques for computational chemistry: The cFOUR program package, *J. Chem. Phys.* **152**, 214108 (2020).
- [87] J. E. Sansonetti and W. C. Martin, Handbook of Basic Atomic Spectroscopic Data, *J. Phys. Chem. Ref. Data* **34**, 1559 (2005).
- [88] K. Balasubramanian, Relativistic configuration interaction calculations of the low-lying states of TlF, *J. Chem. Phys.* **82**, 3741 (1985).
- [89] W. Zou and W. Liu, Comprehensive *ab initio* calculation and simulation on the low-lying electronic states of TlX (X = F, Cl, Br, I, and At), *J. Comput. Chem.* **30**, 524 (2009).
- [90] Y. Liu, X. Yuan, L. Xiao, H. Xu, and B. Yan, Electronic structure and spectroscopy of the low-lying electronic states of thallium fluoride: MRCI+Q study including spin-orbit coupling, *J. Quant. Spectrosc. Radiat. Transf.* **243**, 106817 (2020).
- [91] U. Kaldor, The Fock space coupled cluster method: theory and application, *Theor. Chim. Acta* **80**, 427 (1991).
- [92] L. Visscher, E. Eliav, and U. Kaldor, Formulation and implementation of the relativistic Fock-space coupled cluster method for molecules, *J. Chem. Phys.* **115**, 9720 (2001).
- [93] E. Eliav, A. Borschevsky, A. Zaitsevskii, A. V. Oleynichenko, and U. Kaldor, Relativistic Fock-space coupled cluster method: theory and recent applications, in *Reference Module in Chemistry, Molecular Sciences and Chemical Engineering* (Elsevier, 2022).
- [94] A. Zaitsevskii, N. S. Mosyagin, A. V. Oleynichenko, and E. Eliav, Generalized relativistic small-core pseudopotentials accounting for quantum electrodynamic effects: Construction and pilot applications, *Int. J. Quantum Chem.* **123**, e27077 (2022).
- [95] T. Isaev, A. Zaitsevskii, A. Oleynichenko, E. Eliav, A. Breier, T. Giesen, R. Garcia Ruiz, and R. Berger, Ab initio study and assignment of electronic states in molecular RaCl, *J. Quant. Spectrosc. Radiat. Transf.* **269**, 107649 (2021).
- [96] A. Zaitsevskii, L. V. Skripnikov, N. S. Mosyagin, T. Isaev, R. Berger, A. A. Breier, and T. F. Giesen, Accurate ab initio calculations of RaF electronic structure appeal to more laser-spectroscopical measurements, *J. Chem. Phys.* **156**, 044306 (2022).
- [97] A. V. Zaitsevskii, A. V. Oleynichenko, and E. Eliav, Theoretical molecular spectroscopy of actinide compounds: The ThO molecule (2023), [arXiv:arXiv:2304.13435](https://arxiv.org/abs/2304.13435) [physics.chem-ph].
- [98] A. N. Petrov, N. S. Mosyagin, A. V. Titov, and I. I. Tupitsyn, Accounting for the Breit interaction in relativistic effective core potential calculations of actinides, *J. Phys. B* **37**, 4621 (2004).
- [99] A. V. Oleynichenko, A. Zaitsevskii, N. S. Mosyagin, A. N. Petrov, E. Eliav, and A. V. Titov, LIB-GRPP: A library for the evaluation of molecular integrals of the generalized relativistic pseudopotential operator over Gaussian functions, *Symmetry* **15**, 10.3390/sym15010197 (2023).
- [100] V. M. Shabaev, I. I. Tupitsyn, and V. A. Yerokhin, QEDMOD: Fortran program for calculating the model Lamb-shift operator, *Comput. Phys. Commun.* **223**, 69 (2018).
- [101] Generalized relativistic pseudopotentials (see <http://>



- [qchem.pnpi.spb.ru/recp](http://qchem.pnpi.spb.ru/recp)) (accessed on 26 April 2023).
- [102] N. S. Mosyagin, A. V. Oleynichenko, A. Zaitsevskii, A. V. Kudrin, E. A. Pazyuk, and A. V. Stolyarov, Ab initio relativistic treatment of the  $a^3\Pi - X^1\Sigma^+$ ,  $a'^3\Sigma^+ - X^1\Sigma^+$  and  $A^1\Pi - X^1\Sigma^+$  systems of the CO molecule, *J. Quant. Spectrosc. Radiat. Transf.* **263**, 107532 (2021).
- [103] S. A. Blundell, W. R. Johnson, and J. Sapirstein, Relativistic all-order calculations of energies and matrix elements in cesium, *Phys. Rev. A* **43**, 3407 (1991).
- [104] M. S. Safronova, W. R. Johnson, and A. Derevianko, Relativistic many-body calculations of energy levels, hyperfine constants, electric-dipole matrix elements, and static polarizabilities for alkali-metal atoms, *Phys. Rev. A* **60**, 4476 (1999).
- [105] G. Gopakumar, H. Merlitz, R. K. Chaudhuri, B. P. Das, U. S. Mahapatra, and D. Mukherjee, Electric dipole and quadrupole transition amplitudes for  $Ba^+$  using the relativistic coupled-cluster method, *Phys. Rev. A* **66**, 032505 (2002).
- [106] B. K. Sahoo, S. Majumder, H. Merlitz, R. Chaudhuri, B. P. Das, and D. Mukherjee, Electric dipole transition amplitudes for  $^{207}Pb^+$ , *J. Phys. B: At. Mol. Opt. Phys.* **39**, 355 (2005).
- [107] H. B. Tran Tan and A. Derevianko, Precision theoretical determination of electric-dipole matrix elements in atomic cesium, *Phys. Rev. A* **107**, 042809 (2023).
- [108] A. V. Zaitsevskii, L. V. Skripnikov, A. V. Kudrin, A. V. Oleynichenko, E. Eliav, and A. V. Stolyarov, Electronic transition dipole moments in relativistic coupled-cluster theory: the finite-field method, *Opt. Spectrosc.* **124**, 451 (2018).
- [109] A. Zaitsevskii, A. V. Oleynichenko, and E. Eliav, Finite-field calculations of transition properties by the Fock space relativistic coupled cluster method: transitions between different Fock space sectors, *Symmetry* **12**, 1845 (2020).
- [110] V. Krumins, A. Kruzins, M. Tamanis, R. Ferber, A. Pashov, A. V. Oleynichenko, A. Zaitsevskii, E. A. Pazyuk, and A. V. Stolyarov, The branching ratio of intercombination  $A^1\Sigma^+ \sim b^3\Pi \rightarrow a^3\Sigma^+/X^1\Sigma^+$  transitions in the RbCs molecule: measurements and calculations, *J. Quant. Spectrosc. Radiat. Transf.* **256**, 107291 (2020).
- [111] A. Kruzins, V. Krumins, M. Tamanis, R. Ferber, A. V. Oleynichenko, A. Zaitsevskii, E. A. Pazyuk, and A. V. Stolyarov, Fourier-transform spectroscopy and relativistic electronic structure calculation on the  $e^3\Sigma^+$  state of KCs, *J. Quant. Spectrosc. Radiat. Transf.* **276**, 107902 (2021).
- [112] J. Tellinghuisen, A simple sum rule for total radiative decay rates in diatomics, *Chem. Phys. Lett.* **105**, 241 (1984).
- [113] LIBGRPP, a library for the evaluation of molecular integrals of the generalized relativistic pseudopotential operator (GRPP) over Gaussian functions. (see <https://github.com/aoleynichenko/libgrpp>) (accessed on 26 April 2023).
- [114] A. Oleynichenko, A. Zaitsevskii, and E. Eliav, (2021), EXP-T, an extensible code for Fock space relativistic coupled cluster calculations (see <http://www.qchem.pnpi.spb.ru/exp-t>).
- [115] A. V. Oleynichenko, A. Zaitsevskii, and E. Eliav, Towards high performance relativistic electronic structure modelling: the EXP-T program package, in *Supercomputing*, Vol. 1331, edited by V. Voevodin and S. Sobolev (Springer International Publishing, Cham, 2020) pp. 375–386.
- [116] L. V. Skripnikov, Combined 4-component and relativistic pseudopotential study of ThO for the electron electric dipole moment search, *J. Chem. Phys.* **145**, 214301 (2016).
- [117] D. Sundholm, VIBROT, <http://www.chem.helsinki.fi/~sundholm/software/GPL/>.
- [118] M. Denis, M. S. Norby, H. J. A. Jensen, A. S. P. Gomes, M. K. Nayak, S. Knecht, and T. Fleig, Theoretical study on  $ThF^+$ , a prospective system in search of time-reversal violation, *New J. Phys.* **17**, 043005 (2015).
- [119] H. Lefebvre-Brion and R. W. Field, *The Spectra and Dynamics of Diatomic Molecules* (Elsevier, 2004).
- [120] E. A. Pazyuk, A. V. Zaitsevskii, A. V. Stolyarov, M. Tamanis, and R. Ferber, Laser synthesis of ultracold alkali metal dimers: optimization and control, *Russ. Chem. Rev.* **84**, 1001 (2015).
- [121] A. Zaitsevskii, N. S. Mosyagin, A. V. Stolyarov, and E. Eliav, Approximate relativistic coupled-cluster calculations on heavy alkali-metal diatomics: Application to the spin-orbit-coupled  $A^1\Sigma^+$  and  $b^3\Pi$  states of RbCs and  $Cs_2$ , *Phys. Rev. A* **96**, 022516 (2017).
- [122] T. A. Isaev, Direct laser cooling of molecules, *Phys.-Uspekhi* **190**, 313 (2018).
- [123] M. R. Tarbutt, Laser cooling of molecules, *Contemp. Phys.* **59**, 356 (2018).
- [124] M. V. Ivanov, F. H. Bangertner, and A. I. Krylov, Towards a rational design of laser-coolable molecules: insights from equation-of-motion coupled-cluster calculations, *Phys. Chem. Chem. Phys.* **21**, 19447 (2019).
- [125] A. N. Petrov, N. S. Mosyagin, and A. V. Titov, Theoretical study of low-lying electronic terms and transition moments for  $HfF^+$  for the electron EDM search, *Phys. Rev. A* **79**, 012505 (2009).
- [126] A. Leanhardt, J. Bohn, H. Loh, P. Maletinsky, E. Meyer, L. Sinclair, R. Stutz, and E. Cornell, High-resolution spectroscopy on trapped molecular ions in rotating electric fields: A new approach for measuring the electron electric dipole moment, *J. Mol. Spectrosc.* **270**, 1 (2011).
- [127] P. Tecmer and C. E. González-Espinoza, Electron correlation effects of the ThO and ThS molecules in the spinor basis. A relativistic coupled cluster study of ground and excited states properties, *Phys. Chem. Chem. Phys.* **20**, 23424 (2018).
- [128] V. Andreev, D. Ang, D. DeMille, J. Doyle, G. Gabrielse, J. Haefner, N. Hutzler, Z. Lasner, C. Meisenhelder, B. O’Leary, *et al.*, Improved limit on the electric dipole moment of the electron, *Nature* **562**, 355 (2018).
- [129] T. S. Roussy, L. Caldwell, T. Wright, W. B. Cairncross, Y. Shagam, K. B. Ng, N. Schlossberger, S. Y. Park, A. Wang, J. Ye, and E. A. Cornell, A new bound on the electron’s electric dipole moment (2022), [arXiv:2212.11841 \[physics.atom-ph\]](https://arxiv.org/abs/2212.11841).
- [130] D. G. Ang, C. Meisenhelder, C. D. Panda, X. Wu, D. DeMille, J. M. Doyle, and G. Gabrielse, Measurement of the  $H^3\Delta_1$  radiative lifetime in ThO, *Phys. Rev. A* **106**, 022808 (2022).
- [131] K.-K. Ni, H. Loh, M. Grau, K. C. Cossel, J. Ye, and E. A. Cornell, State-specific detection of trapped  $HfF^+$  by photodissociation, *J. Mol. Spectrosc.* **300**, 12 (2014).

- [132] X. Wu, Z. Han, J. Chow, D. G. Ang, C. Meisenhelder, C. D. Panda, E. P. West, G. Gabrielse, J. M. Doyle, and D. DeMille, The metastable  $Q^3\Delta_2$  state of ThO: a new resource for the ACME electron EDM search, [New J. Phys.](#) **22**, 023013 (2020).